Biochimica et Biophysica Acta 1847 (2015) 640–655

Contents lists available at ScienceDirect

Biochimica et Biophysica Acta

journal homepage: www.elsevier.com/locate/bbabio

Functional characteristics of spirilloxanthin and keto-bearing Analogues in light-harvesting LH2 complexes from *Rhodobacter sphaeroides* with a genetically modified carotenoid synthesis pathway

Dariusz M. Niedzwiedzki [a,*], Preston L. Dilbeck [b], Qun Tang [c], David J. Mothersole [d,1], Elizabeth C. Martin [d], David F. Bocian [c], Dewey Holten [b], C. Neil Hunter [d]

[a] Photosynthetic Antenna Research Center, Washington University, St. Louis, MO 63130, USA
[b] Department of Chemistry, Washington University, St. Louis, MO 63130, USA
[c] Department of Chemistry, University of California Riverside, Riverside, CA 92521, USA
[d] Department of Molecular Biology and Biotechnology, University of Sheffield, Sheffield S10 2TN, UK

ARTICLE INFO

Article history:
Received 23 February 2015
Received in revised form 1 April 2015
Accepted 3 April 2015
Available online 11 April 2015

Keywords:
LH2
Carotenoid
Energy transfer
Spirilloxanthin
Diketospirilloxanthin
Keto-carotenoid

ABSTRACT

Light-harvesting 2 (LH2) complexes from a genetically modified strain of the purple photosynthetic bacterium *Rhodobacter* (*Rba.*) *sphaeroides* were studied using static and ultrafast optical methods and resonance Raman spectroscopy. Carotenoid synthesis in the *Rba. sphaeroides* strain was engineered to redirect carotenoid production away from spheroidene into the spirilloxanthin synthesis pathway. The strain assembles LH2 antennas with substantial amounts of spirilloxanthin (total double-bond conjugation length $N = 13$) if grown anaerobically and of keto-bearing long-chain analogs [2-ketoanhydrorhodovibrin ($N = 13$), 2-ketospirilloxanthin ($N = 14$) and 2,2′-diketospirilloxanthin ($N = 15$)] if grown semi-aerobically (with ratios that depend on growth conditions). We present the photophysical, electronic, and vibrational properties of these carotenoids, both isolated in organic media and assembled within LH2 complexes. Measurements of excited-state energy transfer to the array of excitonically coupled bacteriochlorophyll *a* molecules (B850) show that the mean lifetime of the first singlet excited state (S_1) of the long-chain ($N \geq 13$) carotenoids does not change appreciably between organic media and the protein environment. In each case, the S_1 state appears to lie lower in energy than that of B850. The energy-transfer yield is ~0.4 in LH2 (from the strain grown aerobically or semi-aerobically), which is less than half that achieved for LH2 that contains short-chain ($N \leq 11$) analogues. Collectively, the results suggest that the S_1 excited state of the long-chain ($N \geq 13$) carotenoids participates little if at all in carotenoid-to-BChl *a* energy transfer, which occurs predominantly via the carotenoid S_2 excited state in these antennas.

1. Introduction

The antennas of many purple photosynthetic bacteria consist of two types of light-harvesting (LH) complex, LH1 and LH2. LH2 is a peripheral pigment-protein that absorbs light and transfers excitation energy to LH1, which is closely associated with the reaction center, the ultimate trap for the harvested excitation energy. High resolution structures of LH2 complexes from two bacterial species, *Rhodopseudomonas* (*Rps.*) *acidophila* strain 10050 and *Phaeospirillum* (*Phs.*) *molischianum*, have been determined using X-ray crystallography [1–4]. The antennas have a circular structure consisting of either eight or nine identical protein subunits, each of which is a heterodimer of α and β polypeptides that span the photosynthetic membrane. Each αβ-protein subunit accommodates three bacteriochlorophyll *a* (BChl *a*) and one carotenoid. The macrocycles of two BChl *a* of each subunit are perpendicular to the membrane plane and are electronically (excitonically) coupled to one another and to the pairs from adjacent subunits. These interactions produce a ring-like array of closely-spaced BChl *a* (B850) that has its lowest energy absorption band (the Q_y band) at ~850 nm. The remaining monomeric BChl *a* molecules (B800), one from each subunit, lie parallel to the membrane plane and between polypeptides of adjacent subunits, and have their Q_y band at ~800 nm [1–3].

Abbreviations: ACN, acetonitrile; BChl *a*, bacteriochlorophyll *a*; EADS, evolution-associated difference spectra; ESA, excited-state absorption; FWHM, full width at half maximum; GSB, bleaching of a ground-state-absorption profile; HEPES, 4-(2-hydroxyethyl)-1-piperazineethanesulfonic acid; HPLC, high-performance liquid chromatography; IRF, instrument response function; LDAO, lauryldimethylamine-oxide; LH1, light-harvesting 1 complex; LH2, light-harvesting 2 complex; *n*-hex, *n*-hexane; 2-MTHF, 2-methyltetrahydrofuran; VIS, visible; NIR, near infrared; *Rba*, *Rhodobacter*; *Rps*, *Rhodopseudomonas*; *Rsp*, *Rhodospirillum*; *Phs*, *Phaeospirillum*; *P*, *Pantoea*; TA, transient absorption; RT, room temperature; THF, tetrahydrofuran; Tris, tris(hydroxymethyl)aminomethane; RR, resonance Raman

* Corresponding author.
E-mail address: niedzwiedzki@wustl.edu (D.M. Niedzwiedzki).
[1] Present address: Marine Biology Section, Department of Biology, University of Copenhagen, Strandpromenaden 5, DK-3000 Helsingør, Denmark.

http://dx.doi.org/10.1016/j.bbabio.2015.04.001
0005-2728/

Carotenoids play a dual role in purple bacterial antennas. They assist in light harvesting by absorbing photons in a spectral range (450–550 nm) that is mainly inaccessible to BChl *a*. The excited carotenoid then transfers energy to the BChl *a* species (B800 or B850 in LH2), hereafter denoted Car → BChl energy transfer, with efficiency $\Phi_{Car \rightarrow BChl}$. Carotenoids also play a photoprotective role in efficiently quenching the triplet excited state of the BChl *a*, which otherwise may produce deleterious reactive oxygen species [5]. It has been reported that the propensity for quenching of BChl *a* triplet states in LH1 or LH2 appears to be independent of the type of carotenoid present [6], although a recent study shows that spheroidenone has some unique attributes in this respect, when bound within the LH1 antenna of *Rba. sphaeroides* [7].

$\Phi_{Car \rightarrow BChl}$ varies between different purple bacterial species, but the reasons for this variability are not fully delineated. Among the many contributing factors are the excited-state properties of the carotenoid (e.g., energy and lifetime), the orientation and distance of the carotenoid with respect to the neighboring BChl *a*, and the double-bond conjugation length, and therefore more extended π-electron system, of the carotenoid. For simplicity, the total number of double bonds in the carotenoid conjugation pathway will be designated *N*, reflecting the sum of the contributing C═C bonds ($N_{C=C}$) and C═O bonds ($N_{C=O}$). Prior studies have suggested that terminally attached keto groups ($N_{C=O}$) may not contribute as much as backbone carbons ($N_{C=C}$) to the effective conjugation length [8,9].

Previous studies on LH2 have shown that $\Phi_{Car \rightarrow BChl}$ is greater for carotenoids with lower *N* values. LH2 from the *Rba. sphaeroides* G1C mutant that incorporates neurosporene ($N = 9$) has $\Phi_{Car \rightarrow BChl}$ ~ 90% [8,10,11]. LH2 from wild-type *Rba. sphaeroides* (2.4.1), which contains spheroidene ($N = 10$) when grown photosynthetically (anaerobically) and spheroidenone ($N = 11$, $N_{C=C} = 10$, $N_{C=O} = 1$) when grown semi-aerobically has $\Phi_{Car \rightarrow BChl}$ ~ 99% [8]. However, a previous study of a *Rba. sphaeroides* strain genetically engineered to produce the $N = 11$ carotenoid lycopene found $\Phi_{Car \rightarrow BChl}$ ~ 54% for lycopene–LH2 complexes purified from this strain [12,13]. Similarly, LH2 from *Rps. acidophila* 10050 that contains rhodopin glucoside ($N = 11$) has $\Phi_{Car \rightarrow BChl}$ ~ 55% [8,10,11]. An even lower $\Phi_{Car \rightarrow BChl}$ of 30–40% has been obtained for the LH2 complexes from purple sulfur bacteria such as *Thermochromatium tepidum* and *Allochromatium vinosum* [14,15]. The latter two LH2 complexes combine up to five different carotenoids with conjugation lengths in the range 11–13, with ratios that depend on the growth light conditions [15].

Attempts to isolate the impact of individual factors on $\Phi_{Car \rightarrow BChl}$ have been hindered by the limited number of different carotenoids that can be incorporated into LH2 of a given bacterial species. Carotenoid function could vary between species due to differences such as precise LH2 structures and local/global electrostatics derived from non-identical amino-acid sequences. Genetic engineering of the carotenoid synthesis pathway of *Rba. sphaeroides* [16] offers some advantages by providing a set of LH2 and RC–LH1–PufX complexes that incorporate diverse carotenoids with $N = 9$–15, while each type of complex has the same polypeptides and associated architectural and electrostatic characteristics [17]. The series of LH2 complexes analyzed in the present study, and the analogous RC–LH1–PufX set, provide new vehicles for investigating $\Phi_{Car \rightarrow BChl}$ and associated energy-transfer dynamics in bacterial light-harvesting systems. Initial static spectroscopic studies on this engineered set of *Rba. sphaeroides* of LH2 antennas revealed the general trend of decreasing energy-transfer efficiency with increasing double-bond number for the primary carotenoid produced ($\Phi_{Car \rightarrow BChl}$, *N*): neurosporene (94%, 9), spheroidene (96%, 10), spheroidenone (95%, 11), lycopene (64%, 11), rhodopin (62%, 11), spirilloxanthin (39%, 13), and diketospirilloxanthin (35%, 15) [17].

The present work greatly expands the scope of characterization to include static and ultrafast optical measurements and resonance Raman (RR) studies. The investigations focus on LH2 complexes from the *Rba. sphaeroides crtI::crtI*^{PA} strain, which produces large quantities of the longest-chain carotenoids ($N = 13$ to 15) found thus far in antennas from the purple photosynthetic bacteria (Fig. 1). This strain contains the four-step phytoene desaturase from *Pantoea* (*P.*) *agglomerans*, which feeds carotenoid production into the spirilloxanthin pathway, rather than the native three-step phytoene desaturase that directs carotenoid production along the spheroidene synthesis pathway [17]. Carotenoid production in *crtI::crtI*^{Pa} affords LH2 complexes with carotenoids with conjugation lengths up to spirilloxanthin ($N = 13$, $N_{C=C} = 13$, $N_{C=O} = 0$) when grown under photosynthetic (anaerobic) conditions; smaller amounts of other carotenoids including anhydrorhodovibrin ($N = 12$, $N_{C=C} = 12$, $N_{C=O} = 0$) are also present. When the same strain is grown semi-aerobically, terminal keto groups are added to the carotenoid carbon–carbon-bond backbone, yielding 2-ketoanhydrorhodovibrin ($N = 13$, $N_{C=C} = 12$, $N_{C=O} = 1$), 2-ketospirilloxantion ($N = 14$, $N_{C=C} = 13$, $N_{C=O} = 1$) and 2,2′-diketospirilloxanthin ($N = 15$, $N_{C=C} = 13$, $N_{C=O} = 2$). [Hereafter, the long-chain keto-bearing carotenoids will be referred to simply as ketoanhydrorhodovibrin, ketospirilloxanthin and diketospirilloxanthin.] The ratios of keto-bearing carotenoids (and shorter analogues) depend on growth conditions, specifically the extent of oxygenation of the culture.

LH2 antennas from aerobically or anaerobically grown *Rba. sphaeroides crtI::crtI*^{PA} are of particular interest among the entire set of engineered strains [17] because, aside from LH2 complexes from purple sulfur bacteria that have small quantities of carotenoids with $N = 12$ or 13 [15,18,19], no other LH2 complexes are known to preferentially bind (keto-)carotenoids with such long conjugation lengths ($N \geq 13$). To assess the impact of high *N* value carotenoids on the functional properties of these LH2 complexes, the carotenoid electronic, vibrational, and excited-state properties as well as Car → BChl energy transfer were examined using static and ultrafast optical techniques (at room temperature and 77 K) and RR spectroscopy. In addition, the spectral and excited-state properties (energies, lifetimes) of ketoanhydrorhodovibrin, ketospirilloxanthin and diketospirilloxanthin were studied in representative organic solvents and compared with the properties of the carotenoids within LH2.

2. Materials and methods

2.1. Rba. sphaeroides strains and growth conditions

The *crtI::crtI*^{Pa} strain of *Rba. sphaeroides* was constructed and grown either anaerobically or semi-aerobically as described by Chi et al. [17]. After reaching stationary stage the cultures were harvested and pelleted by centrifugation.

2.2. Isolation and purification of LH2

Pelleted bacterial cells were resuspended in 20 mM tris(hydroxymethyl)-aminomethane (Tris) buffer (pH = 8.0) and the membranes were released by ultrasonication and then pelleted by centrifugation. Subsequently, the pellet was resuspended in 20 mM Tris buffer (pH = 8.0) to $OD_{850} \approx 20$ (1 cm path) and mixed with lauryldimethylamine-oxide (LDAO) to a final concentration of ~0.5% for 20 min at room temperature (RT). The insoluble material was pelleted by centrifugation. Final purification of the complexes was carried out using an anion exchange chromatographic column (Q Sepharose High Performance, GE Healthcare) equilibrated with 20 mM Tris buffer (pH = 8.0) with 0.06% LDAO by applying 50 mM gradient steps of NaCl from 150 and 500 mM. The protein-containing fraction was eluted with 300–400 mM NaCl. Samples for 77 K studies were resuspended in a 50:50 (v/v) glycerol:buffer mixture.

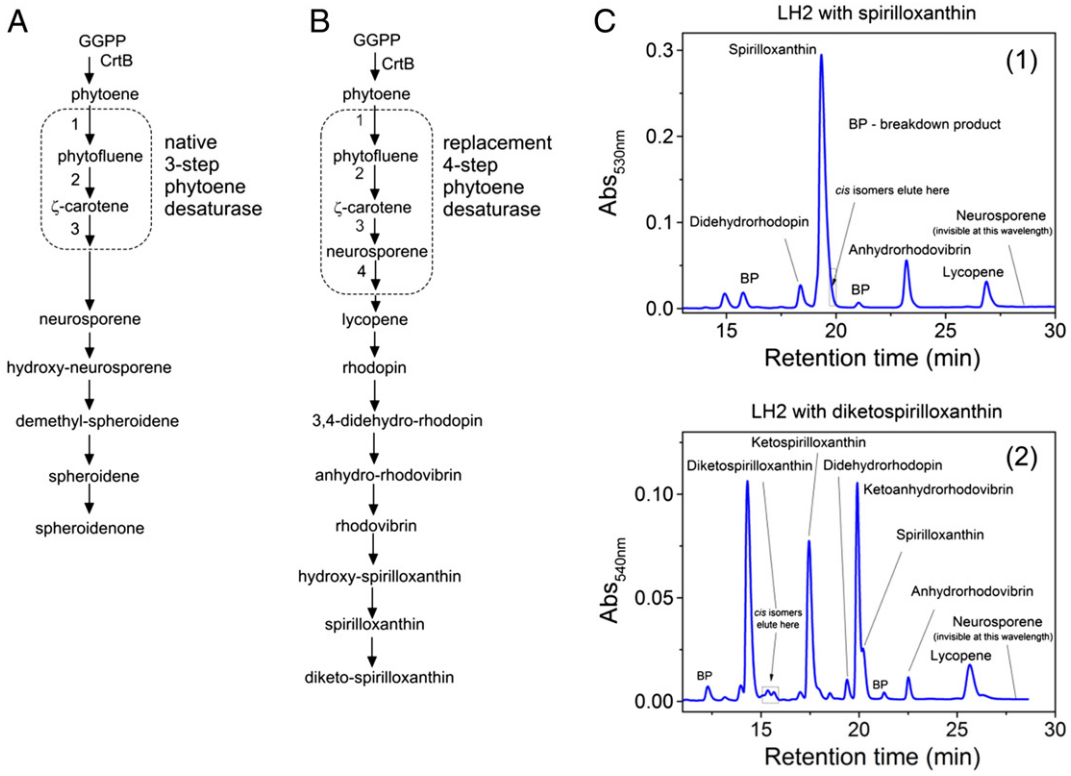

Fig. 1. (A) The spheroidene/spheroidenone carotenoid biosynthesis pathway typical of *Rba. sphaeroides*. The three reactions catalyzed by phytoene desaturase (CrtI) are shown within the dashed outline. (B) The spirilloxanthin pathway; the four desaturation reactions catalyzed by the replacement phytoene desaturase are shown within the dashed outline. (C) Representative chromatograms of the pigment extracts from (1) the spirilloxanthin containing LH2 recorded at 530 nm and (2) diketospirilloxanthin recorded at 540 nm. In both cases, the wavelength corresponds to the (0–0) vibronic band of the carotenoid absorption in the HPLC eluent and thus the trace does not reflect actual ratios of all carotenoids present. BP are "breakdown products", which are very minor components that have unusual absorption spectra and are most probably breakdown/side products of the extraction process.

2.3. Purification of long-chain keto-bearing carotenoids and analysis of LH2 carotenoid content

Carotenoids ketoanhydrorhodovibrin, ketospirilloxanthin and diketospirilloxanthin were extracted from pelleted bacterial cells using a technical grade methanol/acetone (1/1, v/v) mixture. The extract was injected into an Agilent 1100 high-performance liquid chromatography (HPLC) system employing a Zorbax Eclipse XDB-C18 reverse phase column (250 mm × 4.6 mm) and eluted using HPLC grade acetonitrile/tetrahydrofuran (ACN/THF) (95/5, v/v) mixture as a mobile phase with a 1.5 ml min^{-1} flow rate. For analysis of LH2 carotenoid content, the pigment extract from the LH2 was injected into the same HPLC setup programmed for a gradient mobile phase of 100% ACN to 60/40 ACN/THF (v/v) within 30 min. Carotenoid identities are based on the HPLC and mass spectroscopy analysis of the pigment content of these LH2 complexes as described in Chi et al. [17]. The identification of purified carotenoids was similarly made.

2.4. Steady-state and femtosecond time-resolved absorption spectroscopy

Time-resolved pump-probe absorption experiments were carried out using a Helios femtosecond transient absorption (TA) spectrometer (Ultrafast Systems LCC, Sarasota, FL) coupled to a Spectra-Physics femtosecond laser system described previously [15]. Before TA measurements of the LH2 complexes the regular buffer was replaced with D_2O-based buffer to enhance transparency in the near-infrared (NIR) region. For preferential excitation of the LH2-bound spirilloxanthin, the excitation wavelength was set to 555 nm. For diketospirilloxanthin the excitation wavelengths (and medium, temperature) were chosen as follows: 560 nm (*n*-hexane (*n*-hex), RT), 600 nm (2-MTHF, 77 K), 542 nm (LH2, RT) and 560 nm (LH2, 77 K). For ketospirilloxanthin and ketoanhydrorhodovibrin (in *n*-hex at RT), the excitation wavelengths were 550 nm and 535 nm, respectively. For the carotenoids in organic solvents, the energy of the pump beam was set to 500 nJ in a spot size of 1 mm diameter, corresponding to an intensity of ~2×10^{14} photons/cm^2. For carotenoids in the LH2 complexes, the energy of the pump was lowered to 200 nJ (to minimize the possibility of excited-state annihilation in the BChl *a* array, B850) corresponding to an intensity of ~7×10^{13} photons/cm^2. All steady-state absorption measurements were performed using Shimadzu UV-1800 spectrophotometer. For low temperature measurements of diketospirilloxanthin, the purified pigment was dissolved in spectroscopic grade 2-MTHF, transferred to a 1 cm square cryogenic quartz cuvette (NSG Precision Cells, Inc) and frozen in the SVP100 liquid nitrogen cryostat from Janis (Woburn, MA). The optical density (OD) of the sample was set to ~0.5 at the maximum of carotenoid absorption band. For low temperature measurements of the LH2 proteins the buffer was mixed with glycerol in 1:1 (v/v) ratio, transferred to a 1 cm square plastic cuvette and frozen in the above-mentioned cryostat. Fluorescence and fluorescence excitation spectra were acquired at RT using a Horiba-Spex Nanolog fluorometer with 2–4 nm excitation and detection bandwidths and were corrected for the instrument spectral response. Samples had an OD ≤ 0.1 at the excitation and emission wavelengths to avoid front-face and inner-filter effects.

2.5. Data processing and fitting

Group velocity dispersion in the TA datasets was corrected using Surface Explorer Pro software (v.2.3) (Ultrafast Systems LCC) by building a dispersion correction curve from a set of initial times of transient signals obtained from single wavelength fits of representative kinetics. Global analysis of the TA datasets was performed using a modified version of ASUfit 3.0, program provided by Dr. Evaldas Katilius at Arizona

State University. The full width at half maximum (FWHM) of a temporal response function was assumed to be ~150 fs for all the measurements in the visible (VIS) spectral range and ~200 fs in the NIR spectral range and was used as a fixed parameter in the fitting procedures. In an idealized scenario the TA data should be fitted with anticipated, realistic kinetic model mimicking the true decay pathways following excitation. However, for structurally complicated systems like LH2 the precise decay scheme is complex and uncertain. Alternatively the datasets may be fitted with a non-branching, sequential, irreversible scheme A → B → C → D, where arrows represent increasingly slower mono-exponential decays, with time constants corresponding to lifetimes of the transient species A, B, C, D. The spectral profiles of these species are termed Evolution-Associated Difference Spectra (EADS) [20]. EADS do not necessarily correspond to a particular process, excited state, or individual species (carotenoid or the BChl *a* entities B800 or B850); however, the EADS help visualize the time evolution of the spectral features of the whole system (e.g., LH2). This type of fitting was applied to all TA data in this work.

2.6. RR spectroscopy

The RR spectra of the isolated carotenoids were obtained at 4 °C in THF solutions with the samples contained in 1 mm diameter capillary tubes. The spectra of the carotenoids in the LH2 complexes were obtained at 4 °C in buffer solutions (either 20 mM Tris at pH 8.0 with 0.06% LDAO and 400 mM NaCl or 4-(2-hydroxyethyl)-1-piperazineethanesulfonic acid (HEPES) at pH 7.5 with 0.03% n-dodecyl-beta-D-maltoside) with the samples contained in 1 mm diameter capillary tubes.

The RR spectra were acquired with a triple spectrograph (Spex 1877) equipped with holographically etched 1800 groove/mm gratings in the third stage. A UV-enhanced charge-coupled device was used as the detector (Princeton Instruments LN/CCD equipped with an EEV1152-UV chip). The excitation wavelength of 532 nm was provided by the discrete output of a diode-pumped solid-state laser (Coherent Verdi-V6). The laser power was typically 5–6 mW; the beam diameter was ~0.5 mm. The scattered light was collected at 90° using a 50 mm f/1.4 Cannon camera lens. The spectra were acquired with 1–2 h of signal averaging (20 × 180 s to 40 × 180 s scans). The spectral resolution was ~2 cm^{-1} at a Raman shift of 200 cm^{-1}. The spectra data were calibrated using the known frequencies of indene.

3. Results

3.1. Analysis of carotenoid content in the LH2 complexes

Fig. 1A shows the native carotenoid biosynthesis pathway for *Rba. sphaeroides* and the altered pathway leading to spirilloxanthin and diketospirilloxanthin (Fig. 1B), resulting from a gene replacement that swaps the 3-step phytoene desaturase for a 4-step enzyme. The final step in both pathways (spheroidene/spheroidenone; spirilloxanthin/diketospirilloxanthin) is catalyzed by a monooxygenase, so the oxygen level of the culture determines the extent of this reaction [21,22]. Representative chromatograms of the LH2 from *Rba. sphaeroides crtI::crtI^{Pa}* recorded at 530 nm (anaerobically grown strain) and at 540 nm (semi-aerobically grown strain) are shown in Fig. 1C. The chromatograms were analyzed using the simplifying assumption that all carotenoids present have very similar molar extinction coefficients (ε_{mol}) at their absorption maximum in the solvent mixture used for the HPLC runs. This is reasonable because most open-chain carotenoids from purple photosynthetic bacteria have ε_{mol} in range of 145,000–160,000 M^{-1} cm^{-1} at their (1,0) vibronic band [23]. The carotenoid content of the samples is summarized in Table 1. The major carotenoids in the LH2 complex from anaerobically grown bacterium are spirilloxanthin (N = 13, 60%) and anhydrorhodovibrin (N = 12, 15%). The major carotenoids in the LH2 from semi-aerobically grown bacterium are keto-bearing carotenoids with the increased double-bond length and are ketoanhydrorhodovibrin (N = 13, 28%), ketospirilloxanthin (N = 14, 16%), and diketospirilloxanthin (N = 15, 21%).

The chromatograms in Fig. 1 also indicate that the carotenoids all primarily have the all-*trans* configuration, in agreement with the RR data on the isolated carotenoids from the same extracts (vide infra). The *cis* isomers of the carotenoids present elute at the edge of the main chromatographic peaks, as can be seen for spirilloxanthin. The amounts of *cis* isomers present are typical for minor spontaneous, thermal isomerization after extraction from LH2. Thus, there appears to be no or only trace amounts of *cis* isomers of these carotenoids when bound to LH2.

3.2. Absorption spectra of LH2 complexes at RT and at 77 K

Fig. 2A and B show RT and 77 K absorption spectra of LH2 from the *Rba. sphaeroides crtI::crtI^{Pa}* strain grown photosynthetically (anaerobically) or semi-aerobically, respectively. The B800 band (BChl *a* monomers) and B850 band (BChl *a* oligomer) appear at 798 and 849 nm, respectively, in both complexes. Upon lowering the temperature, the B850 band bathochromically shifts 3 nm and the B800/B850 peak-intensity ratio increases from 0.75 to 0.91. These spectral characteristics demonstrate good overall assembly of the BChl *a* molecules into polypeptide matrix [8,24].

The carotenoid absorption contours are more complex and differ with carotenoid content, which for *Rba. sphaeroides crtI::crtI^{Pa}* depends on growth conditions (anaerobic or semi-aerobic) (Table 1). In the case of LH2 that contains primarily spirilloxanthin, the vibronic bands of the carotenoid absorption spectrum (420–580 nm) are clearly resolved even at RT (Fig. 2A). However, for LH2 with keto-bearing carotenoids lowering the temperature to 77 K does not substantially improve the vibronic resolution (Fig. 2B), indicating substantial overlap of the absorption features of the bound pigments. Nonetheless the carotenoid absorption contours can be reconstructed from the spectra of the contributing carotenoids because the positions of the respective (0,0) bands are predictable. Based on previous studies of reconstitution of the LH1 complex from *R. rubrum* with various types of carotenoids and on the LH2 complexes containing only single carotenoid [8,25], the positions of (0,0) absorption bands of the non-ketolated carotenoids are expected to be as follows: spirilloxanthin (~550 nm), anhydrorhodovibrin and didehydrorhodopin (~536 nm), lycopene (~516 nm), and neurosporene (~491 nm). The absorption spectra of keto-bearing counterparts (obtained from HPLC) show that introduction of one terminal C═O group onto a C═C backbone shifts the absorption spectrum by 500 cm^{-1} to lower energy. Therefore, the spectral positions of keto-bearing carotenoids in LH2 from the semi-aerobically grown bacterium are predicted to be as follows: diketospirilloxanthin (~582 nm), ketospirilloxanthin (~565 nm), and ketoanhydrorhodovibrin (~550 nm).

The absorption spectra of the individual carotenoids can be used along with the percent contributions from HPLC (Table 1) to accurately reconstruct (simulate) the observed spectra of both LH2 complexes (Fig. 2C and D). The fidelity of the fits was judged by the difference between the raw LH2 absorption spectrum and the fitted trace, which should mimic the absorption spectrum of the BChl *a* content, which can be seen independently from LH2 that naturally lacks carotenoids [26]. Using the same assumption that in LH2 the peak molar absorptivity (ε_{mol}) is the same for each carotenoid, the percent contribution of each pigment to the total composition based on the spectral reconstruction can be calculated. These values along with the wavelength positions of the (0,0) vibronic bands used are listed in the last four columns of Table 1. The agreement with the carotenoid compositions obtained from the HPLC analysis shown in columns 5 and 6 of the table are excellent. These comparisons demonstrate consistency in the analysis of the carotenoid content of the LH2 complexes under study.

Table 1
Carotenoid content in LH2 from *Rba. sphaeroides crtI::crtI*^{Pa} from HPLC and spectral analysis.[a]

Carotenoid	N[d]	$N_{C=C}$	$N_{C=O}$	HPLC analysis[b] PA grown %	HPLC analysis[b] SA grown %	Spectral reconstruction analysis[c] PA grown %	λ(0,0) (nm)[e]	SA grown %	λ(0,0) (nm)[f]
Neurosporene	9	9	0	4	3	5	491	7	491
Lycopene	11	11	0	13	15	10	517	15	518
Didehydrorhodopin	12	12	0	8	6	17[g]	536	17[g]	536
Anhydrorhodovibrin	12	12	0	15	7	17[g]	536	17[g]	536
Spirilloxanthin	13	13	0	60	4	68	554	5	551
Ketoanhydrorhodovibrin	13	12	1		28			24	554
Ketospirilloxanthin	14	13	1		16			12	568
Diketospirilloxanthin	15	13	2		21			20	584

[a] Strains grown photosynthetically (PS) or semi-aerobically (SA) and LH2 isolated and purified as described in the Materials and methods section.
[b] See Figure S1.
[c] Performed using the simplifying assumption that the carotenoids all have the same peak extinction of the (0,0) band.
[d] The total number of double bonds (C═C and C═O) in the conjugated π-electron system.
[e] Wavelength for the (0,0) band returned from the spectral reconstruction for LH2 from the photosynthetically grown strain.
[f] Wavelength for the (0,0) band returned from the spectral reconstruction for LH2 from the semi-aerobically grown strain.
[g] Combined value for the two carotenoids.

3.3. RR spectra of carotenoids in LH2 and organic media

RR spectra of the isolated carotenoids in THF solutions were obtained for comparison with results for the LH2 complexes (Fig. 3). The ν_1 vibrational energies of the carotenoids in solution are generally consistent with an all-*trans* conformation, in keeping with the HPLC data. The ν_1 energies generally track the conjugation length [27–29]. This point is illustrated by the RR spectra of anhydrorhodovibrin ($N = 12$), spirilloxanthin ($N = 13$), ketoanhydrorhodovibrin ($N = 13$), ketospirilloxanthin, ($N = 14$) and diketospirilloxanthin ($N = 15$) for which ν_1 is found at 1509, 1507, 1507, 1505 and 1501 cm^{-1}, respectively.

Fig. 3 also shows RR spectra of the LH2 complexes from the *Rba. sphaeroides crtI::crtI*^{Pa} strain grown anaerobically (blue) and semi-aerobically (magenta). The breadth of the spectra is consistent with contributions of mixtures of carotenoids. Visually, the general nature of the required mixtures of individual spectra (based on the solution RR data) are consistent with the pigment content (Table 1) and

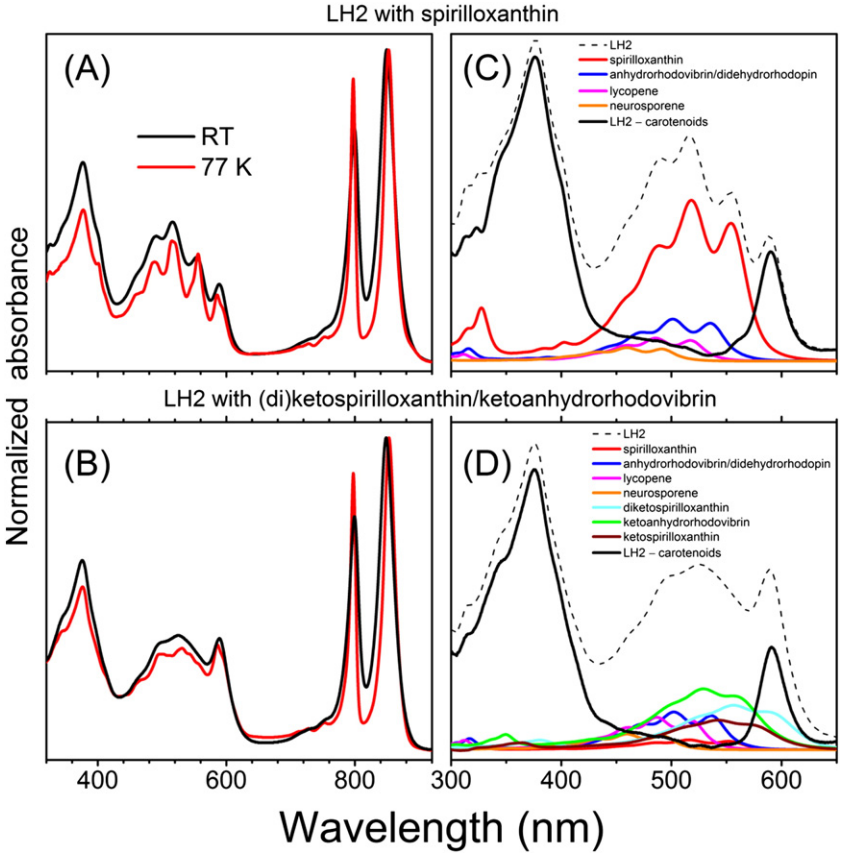

Fig. 2. (A, B) Steady-state absorption spectra of the LH2 complexes containing spirilloxanthin and diketospirilloxanthin (along with other carotenoids) recorded in buffer at RT and in the glycerol/buffer glass at 77 K. The spectra are normalized at the B850 band. (C, D) Spectral reconstruction of the carotenoid absorption contour of LH2 at RT. The actual positions of the absorption spectra of carotenoids show minimal deviation from those expected (see Table 1 for details). The dotted line represents the raw absorption of the LH2. The solid black line is obtained from subtraction of the sum of carotenoid features from the raw LH2 absorption and resembles the anticipated absorption spectrum of BChl *a*.

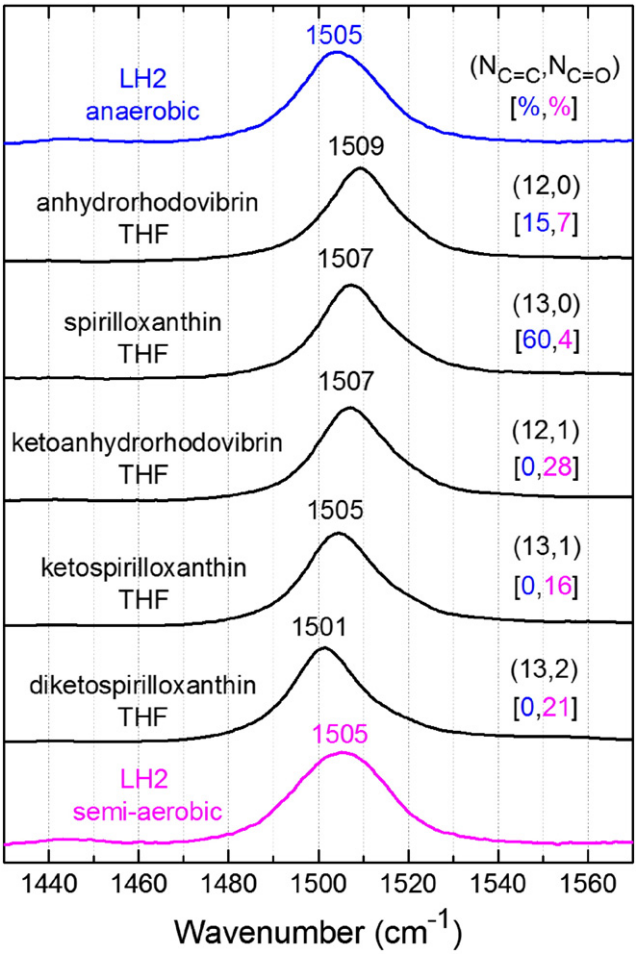

Fig. 3. RR spectra of $N = 12–15$ carotenoids in THF and (as mixtures) in LH2 obtained using $\lambda_{exc} = 532$ nm. The values in round parenthesis give the number of C═C and C═O bonds in the individual carotenoid. The values in square brackets give the percent contribution of the carotenoid.

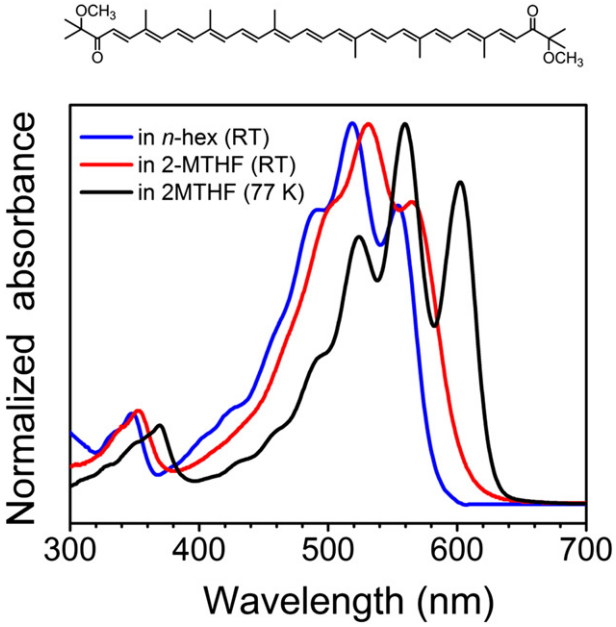

Fig. 4. The chemical structure of diketospirilloxanthin along with its steady-state absorption spectrum in *n*-hex and 2-MTHF at RT and 77 K. The spectra were normalized to their maxima to facilitate comparisons.

expected relative absorption at the 532 nm excitation wavelength seen from the optical spectral reconstructions (Fig. 2C and D). For example, for LH2 from the strain grown anaerobically, the RR spectrum can be understood as deriving from contributions from anhydrorhodovibrin and spirilloxanthin (with a small shift to lower cm^{-1} from the position in THF). In turn, the RR spectrum of LH2 from the strain grown semi-aerobically can be understood in terms of a mixture of ketoanhydrorhodovibrin, ketospirilloxanthin, and diketospirilloxanthin, with perhaps a small contribution from other carotenoids present (Table 1). Spectral fits were not performed because the inclusion of resonance energy denominators (including RR and absorption positions of the individual carotenoids in LH2) entails such a large number of parameters.

3.4. Steady-state and TA studies of long-chain keto-bearing carotenoids

3.4.1. Absorption spectra of diketospirilloxanthin in organic media at RT and 77 K

Steady-state absorption spectra of diketospirilloxanthin are given in Fig. 4. In *n*-hex the (0,0) vibronic band of the $S_0(1^1A_g^-) \rightarrow S_2(1^1B_u^+)$ transition is at 554 nm (18,050 cm^{-1}) and the absorption spectrum peaks at the 518 nm (1,0) vibronic band. The ratio of (0,0) and (1,0) bands is 0.8. A similar spectrum but with small bathochromic shifts is observed upon changing the solvent to the more polarizable and polar 2-MTHF. Upon freezing to 77 K in 2-MTHF, the spectral features are further bathochromically shifted such that the (0–0) vibronic band is at 602 nm (~16,600 cm^{-1}). The vibronic resolution is also enhanced at 77 K.

The temperature induced spectral shift is caused by the large polarizability of 2-MTHF 77 K glass (versus at RT for 2-MTHF and *n*-hex) that energetically stabilizes the S_2 ($1^1B_u^+$) state. The improved vibronic resolution allows a more precise estimate of the spacing of the absorption bands. In general, the vibronic structure of the $S_0(1^1A_g^-) \rightarrow S_2(1^1B_u^+)$ absorption contour of carotenoids can be modeled as combinations of the progressions of two vibrational modes with energies of ~1200 cm^{-1} (totally symmetric C–C stretch) and ~1600 cm^{-1} (totally symmetric C═C stretch) [30]. The spacing between successive pairs of bands in the 77 K absorption spectrum of diketospirilloxanthin (Fig. 1) is ~1280 cm^{-1}, which suggests that the progression is dominated by the totally symmetric C–C stretching vibration.

3.4.2. TA studies of long-chain keto-bearing carotenoids in organic solvents

Fig. 5 panels A–F show TA data for diketospirilloxanthin in *n*-hex at RT. The left stack of panels (A–C) show data in the visible (VIS) region and the right stack of panels (D–F) in the NIR region. The top row of panels (A, D) displays contour plots of the TA data. The middle row of panels (B, E) shows spectra obtained from global analysis (EADS), which employed four components (exponentials) in the VIS and one or two in the NIR because some states/processes contribute significantly to the former and not the latter. The bottom row of panels (C, F) shows representative kinetic profiles and fits using the time constants derived from global analysis, normalized to the amplitude at t = 0. Analogous data for diketospirilloxanthin in 2-MeTHF at 77 K are shown in Figure S1. Similar data were acquired in *n*-hex at RT for the two keto-bearing carotenoids with shorter conjugation lengths. The results for ketospirilloxanthin are shown in Fig. 5 panels G–L and those for ketoanhydrorhodovibrin in Fig. 5 panels M–R.

In the following, the data for diketospirilloxanthin ($N = 15$, $N_{C=C} = 13$, $N_{C=O} = 2$) at the two temperatures are discussed first, followed by the main differences for ketospirilloxanthin ($N = 14$, $N_{C=C} = 13$, $N_{C=O} = 1$) and ketoanhydrorhodovibrin ($N = 13$, $N_{C=C} = 12$, $N_{C=O} = 1$). The key issues are the lifetime and spectral positions (energies) of the transient features associated with the $S_2(1^1B_u^+)$ and $S_1(1^1A_g^-)$ excited states, because these two states are donors for energy transfer

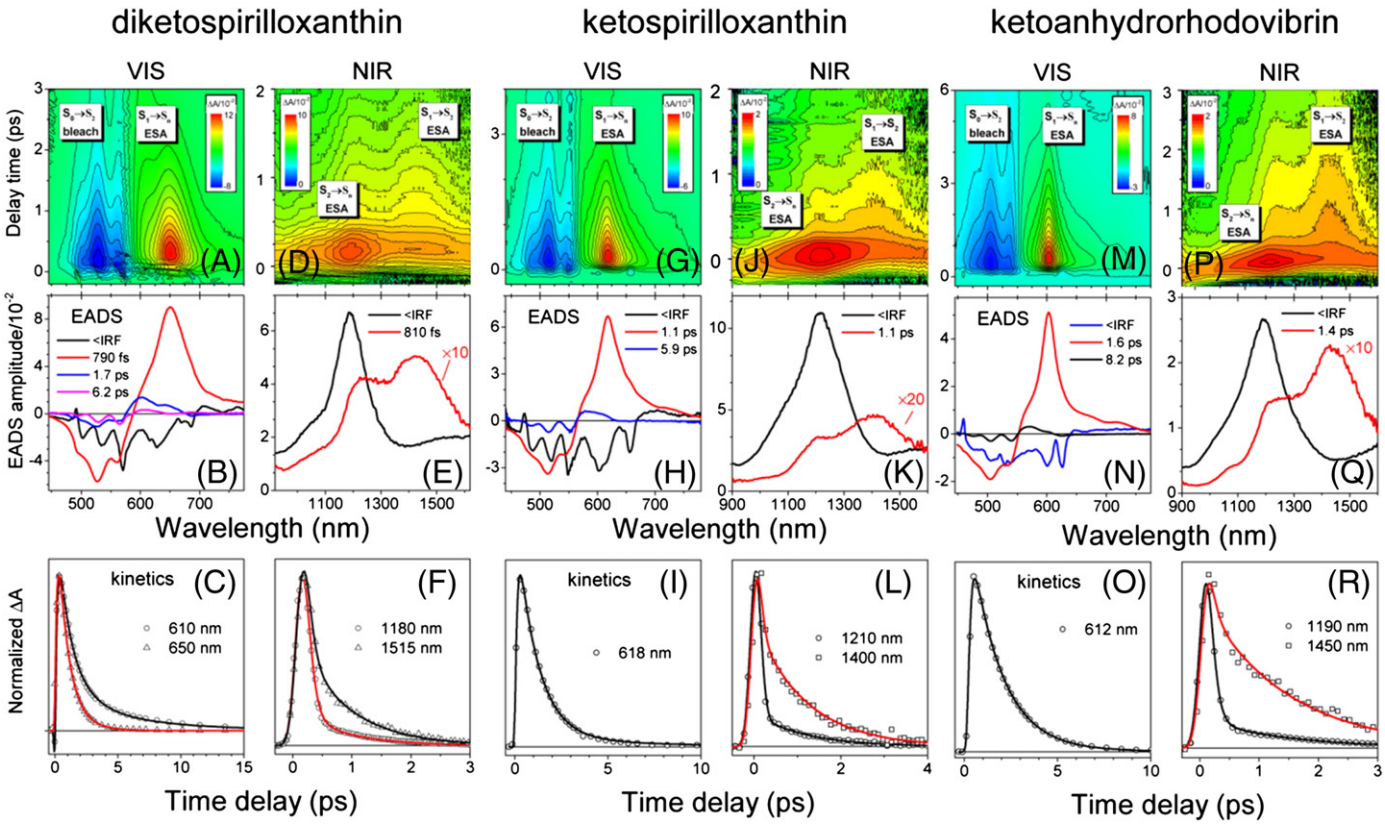

Fig. 5. Transient absorption results for keto-bearing carotenoids diketospirilloxanthin (A–F), ketospirilloxanthin (G–L) and ketoanhydrorhodovibrin (M–R) in *n*-hex at RT in the VIS region (A–C, G–I, M–O) and NIR region (B–E, J–L, P–R) upon excitation at 560 nm (A–F), 550 nm (G–L), or 540 nm (M–R). The top panels show 2D contours, middle panels results of global analysis (EADS) of the data sets, and bottom panels representative kinetic profiles (symbols) and multi-exponential fits using the time constants obtained from global analysis (solid lines), normalized to the same amplitude at t = 0. The dynamics in (C, I, O) shows decay of the S_1 ($2^1A_g^-$) state probed at the S_1 ($2^1A_g^-$) → S_n ESA peak on the short- or long-wavelength-wavelength edge. The profiles in (F, L, R) are for decay of the S_2 ($1^1B_u^+$) state (1180, 1210, 1190 nm) and the S_1 ($2^1A_g^-$) state (1515, 1400, 1450 nm). To enhance visibility of the NIR contours, the ΔA magnitude is shown in logarithmic scale in figures D, J and P.

to the BChl *a* constituents (B800 and B850). The key results are summarized in Table 2.

The spectral changes associated with the $S_2(1^1B_u^+)$ excited state for diketospirilloxanthin and its decay at RT are given by the first EADS in Fig. 5B (VIS) and Fig. 5E (NIR); the data at 77 K are given in Figure S1. The $S_2(1^1B_u^+)$ lifetime is at or below the width of the instrument response function (IRF; 150 fs for VIS and 200 fs for NIR). The spectral signatures of this state are as expected: The spectrum in the VIS includes combined bleaching of the $S_0(1^1A_g^-) \rightarrow S_2(1^1B_u^+)$ ground-state absorption profile (GSB) and stimulated $S_2(1^1B_u^+) \rightarrow S_0(1^1A_g^-)$ emission (with shape somewhat obscured by solvent-response features during the ~100 fs excitation flash). The spectrum in the NIR includes a distinct band at ~1200 nm due to $S_2(2^1A_g^-) \rightarrow S_n$ absorption, in which *n* stands for a higher excited state with A_g-like symmetry [31].

The spectral changes associated with the $S_1(1^1A_g^-)$ excited state and its decay for diketospirilloxanthin are given by the second EADS in Fig. 5B and E (RT) and Figure S1-B and S1-E (77 K). The S_1 ($1^1A_g^-$) lifetime is 800 fs at RT [average of 790 fs (VIS) and 810 fs (NIR)] and lengthens to 1.1 ps at 77 K [average of 1.2 ps (VIS) and 1.0 ps (NIR)]. The spectral signatures (EADS) associated with this state are as expected: the spectrum in the VIS includes a negative feature due to GSB of the $S_0(1^1A_g^-) \rightarrow S_2(1^1B_u^+)$ absorption profile and a positive feature with a maximum at ~650 nm at RT and ~700 nm at 77 K associated with the $S_1(1^1A_g^-) \rightarrow S_n$ excited-state absorption (ESA), in which *n* stands for *n*th excited state(s) with presumed B_u-like symmetry for an allowed transition (see [32,33] for a review). The spectrum in the NIR shows the prominent $S_1(2^1A_g^-) \rightarrow S_2(1^1B_u^+)$ ESA band [34–36]. The ESA band has a maximum at ~1400 nm at RT and shifts bathochromically so much at 77 K that part of the profile is past the NIR probe limit of 1600 nm (Figures S1-D and S1-E).

The impact of cryogenic temperature on the ground- and excited-state absorption features is noteworthy because the spectral positions provide an estimate of the energy of the $S_1(2^1A_g^-)$ excited state (vide infra). The bathochromic shift of the $S_1(2^1A_g^-) \rightarrow S_n$ ESA band from 650 nm at RT to 700 nm at 77 K (i.e., a reduced energy gap between the states) derives from the large polarizability of 2-MTHF glass that energetically stabilizes the S_n state(s). A similar stabilization of the $S_2(1^1B_u^+)$ state underlies the bathochromic shift (554 to 602 nm) of the $S_0(1^1A_g^-) \rightarrow S_2(1^1B_u^+)$ profile in the ground-state absorption spectrum (Fig. 1) and the main $S_1(2^1A_g^-) \rightarrow S_2(1^1B_u^+)$ feature (~1400 nm to >1600 nm) in the ESA spectrum (Figs. 5E and S1-E).

The origin of the two additional EADS components (1.7 and 6.2 ps at RT; 1.6 and 5.6 ps at 77 K) in the VIS data sets for diketospirilloxanthin (Figs. 5B and S1-B) is not clear. Previous TA studies of carotenoids with long conjugation lengths showed similar spectral/kinetic features that were assigned to undefined excited state(s) denoted S*, which were first observed in long-chain analogues of β-carotene [37]. It has been hypothesized that S* is a vibrationally non-equilibrated ground state [37,38], a distinct electronic state in the energy vicinity of $S_1(1^1A_g^-)$ [39], or the $S_1(1^1A_g^-)$ itself but with a twisted configuration [35,40].

The TA for ketospirilloxanthin (Fig. 5 panels G–L) and ketoanhydrorhodovibrin (Fig. 5 panels M–R) in *n*-hex at RT can be similarly analyzed. The key differences from diketospirilloxanthin are two-fold. One is a lengthening of the S_1 lifetime in *n*-hex at RT with a decrease in the number of double bonds in the carotenoid conjugation length: from 0.8 ps for diketospirilloxanthin ($N = 15$,

Table 2
The properties of the S_1 ($2^1A_g^-$) state (energies and lifetimes) of carotenoids found in various LH2 complexes, obtained at various temperatures and environments along with the Car → BChl energy-transfer efficiency.[a]

Carotenoid	N	$N_{C=C}$	$N_{C=O}$	S_2 (cm^{-1}) [nm]	S_1 (cm^{-1}) [nm]	τ_{S1} (ps)	System	$\Phi_{Car \rightarrow BChl}$ (%)[b]	Temp	Ref
Neurosporene	9	9	0	21,300 [469]			*n*-hex		RT	[63]
					14,170 [706]	21–25	v.s.		RT	[35,64,65]
				20,790 [481]	14,400 [694]	35	EPA glass		77 K	[42]
				20,330 [492]	n.d.	1.2	LH2[c]	91	RT	[8]
				20,240 [494]	n.d.	0.9	LH2[c]	91	10 K	[8]
				20,700 [483]			*n*-hex		RT	[34,52]
Spheroidene	10	10	0		13,400 [746]	7–8	v.s.		RT	[34,35,63,66,67]
				20,000 [500]	13,400 [746]	11.5	EPA glass		77 K	[42]
				19,570 [511]	n.d.	1.5	LH2[d]	93	RT	[8]
				19,420 [515]	n.d.	1.5	LH2[d]	88	10 K	[8]
Spheroidenone	11	10	1	19,460 [514]	12,800 [781]	6.0	*n*-hex		RT	[8]
				19,500 [513]	13,000 [769]	6.0	*n*-hex		RT	[55]
				18,070 [553]	n.d.	0.8	LH2[e]	94	RT	[8]
				17,790 [562]	n.d.	0.9	LH2[e]	92	10 K	[8]
				19,160 [522]	n.d.	5.9	EPA glass		77 K	[35]
Rhodopin glucoside	11	11	0	20,000 [500]	12,500 [806]	~4.0	MeOH		RT	[8]
				19,080 [524]	n.d.	3.3	LH2[f]	54	RT	[8]
				18,900 [529]	n.d.	3.6	LH2[f]	52	10 K	[8]
				19,000 [526]	n.d.		*n*-hex		RT	[68]
Spirilloxanthin	13	13	0		11,500 [870]	1.3–1.5	v.s.		RT	[35,39,41,43–45,68]
				18,280 [547]	n.d.	1.7	EPA glass		77 K	[35]
				18,100 [552]	11,430 [875]	2.0	2-MTHF glass		77 K	[42]
				18,040 [554]	11,300 [885]	1.4	LH2[g]	41	RT	This work
				n.d.	n.d.	1.6	LH2[g]		77 K	This work
Ketoanhydrorhodovibrin	13	12	1	18,600 [538]	11,270 [887]	1.5	*n*-hex		RT	This work
Ketospirilloxanthin	14	13	1	18,350 [545]	11,250 [889]	1.1	*n*-hex		RT	This work
Diketospirilloxanthin	15	13	2	18,080 [553]	11,100 [908]	0.8	*n*-hex		RT	This work
				16,610 [602]	11,000 [909]	1.2	2-MTHF glass		77 K	This work
				17,040 [586]	10,500 [952]	1.1	LH2[h]	42	RT	This work
				n.d.	n.d.	1.8	LH2[h]		77 K	This work

[a] n.d. — not determined, EPA — (diethyl ether/isopentane/ethanol, 5/5/2, v/v/v), v.s. — various solvents.
[b] Carotenoid-to-BChl energy-transfer yield obtained from comparison of 1 − T and fluorescence excitation profiles. The values for the new set of engineered *Rba. sphaeroides* mutants obtained in the initial study [17] are as follows ($\Phi_{Car \rightarrow BChl}$, N): neurosporene (94%, 9), spheroidene (96%, 10), spheroidenone (95%, 11), lycopene (64%, 11), rhodopin (62%, 11), spirilloxanthin (39%, 13), and diketospirilloxanthin (35%, 15).
[c] *Rba. sphaeroides* G1C.
[d] *Rba. sphaeroides* 2.4.1 (anaerobic).
[e] *Rba. sphaeroides* 2.4.1 (aerobic).
[f] *Rps. acidophila.*
[g] *Rba. sphaeroides crtI::crtI*^{Pa} (anaerobic).
[h] *Rba. sphaeroides crtI::crtI*^{Pa} (semi-aerobic).

$N_{C=C} = 13$, $N_{C=O} = 2$) to 1.1 ps for ketospirilloxanthin ($N = 14$, $N_{C=C} = 13$, $N_{C=O} = 1$) to 1.5 ps for ketoanhydrorhodovibrin ($N = 13$, $N_{C=C} = 12$, $N_{C=O} = 1$). The latter value is comparable 1.3–1.4 ps reported for spirilloxanthin ($N = 13$, $N_{C=C} = 13$, $N_{C=O} = 0$) in *n*-hex at RT [39,41]. The second major difference for the three keto-bearing carotenoids is a trend of the position of the $S_1(2^1A_g^-) \rightarrow S_2(1^1B_u^+)$ ESA feature in the NIR TA data to a longer wavelength (lower energy) with decreasing number of double bonds in the carotenoid conjugation path (Fig. 2E, K, Q). This trend translates to a shift in the energy of the $S_1(2^1A_g^-)$ state, as described next.

3.4.3. The $S_1(2^1A_g^-)$ state energy of long-chain keto-bearing carotenoids in organic media

The energies of the $S_1(2^1A_g^-)$ and $S_2(1^1B_u^+)$ states have been determined previously for numerous non-carbonyl open-chain carotenoids from purple bacteria from studies at 77 K [15,42]. Such energies have been reported from RT studies of carotenoids with conjugation lengths up to $N = 13$ (spirilloxanthin), including a keto-carotenoid with $N = 11$ (spheroidenone) (Table 2). The data obtained herein (Figs. 4,5 and S1) provide the means to extend analysis of the S_1 energies to both longer conjugation lengths and additional keto-bearing carotenoids. This extension is made possible for ketoanhydrorhodovibrin, ketospirilloxanthin and diketospirilloxanthin because transition wavelengths of ground-state absorption $[S_0(1^1A_g^-) \rightarrow S_2(1^1B_u^+)]$ and excited-state absorption $[S_1(2^1A_g^-) \rightarrow S_2(1^1B_u^+)]$ were measured in the same samples at RT (and both RT and 77 K for diketospirilloxanthin). For diketospirilloxanthin, following conversion of wavelengths to wavenumbers, the $[S_1(2^1A_g^-) \rightarrow S_2(1^1B_u^+)]$ NIR ESA profile (Fig. 5E) was shifted by an energy needed to obtain coincidence with the $[S_0(1^1A_g^-) \rightarrow S_2(1^1B_u^+)]$ ground-state absorption profile (Fig. 2 or 4). This shift is the $S_1(2^1A_g^-)$ energy. A value of 11,100 cm^{-1} is found for diketospirilloxanthin in *n*-hex at RT (Fig. 6A) and 11,000 cm^{-1} in 2-MTHF at 77 K (Figure S2). The same analysis is given in Fig. 6B for ketospirilloxanthin and in Fig. 6C for ketoanhydrorhodovibrin in *n*-hex at RT.

Collectively the results show an increase in $S_1(2^1A_g^-)$ energy (in *n*-hex at RT) with decreasing number of double bonds in the conjugation path. The trend is from 11,100 cm^{-1} for diketospirilloxanthin ($N = 15$, $N_{C=C} = 1\,3$, $N_{C=O} = 2$) to 11,250 cm^{-1} for ketospirilloxanthin ($N = 14$, $N_{C=C} = 13$, $N_{C=O} = 1$) to 11,750 cm^{-1} for ketoanhydrorhodovibrin ($N = 13$, $N_{C=C} = 12$, $N_{C=O} = 1$). The latter values are comparable to the reported value of 11,500 cm^{-1} for spirilloxanthin ($N = 13$, $N_{C=C} = 13$, $N_{C=O} = 0$) in *n*-hex at RT [41]. These data will be analyzed in conjunction with the $S_1(2^1A_g^-)$ energies for shorter-chain carotenoids (Table 2) in the Discussion section.

3.5. Studies of carotenoid electronic and energy-transfer characteristics in LH2 complexes

3.5.1. Car → BChl energy transfer efficiencies in LH2 employing long-chain carotenoids

Fig. 7 shows analysis of $\Phi_{Car \rightarrow BChl}$ using steady-state fluorescence and absorption spectroscopy. Panel A shows results for *Rba. sphaeroides crtI::crtI*^{Pa} grown anaerobically and panel B gives data for the same

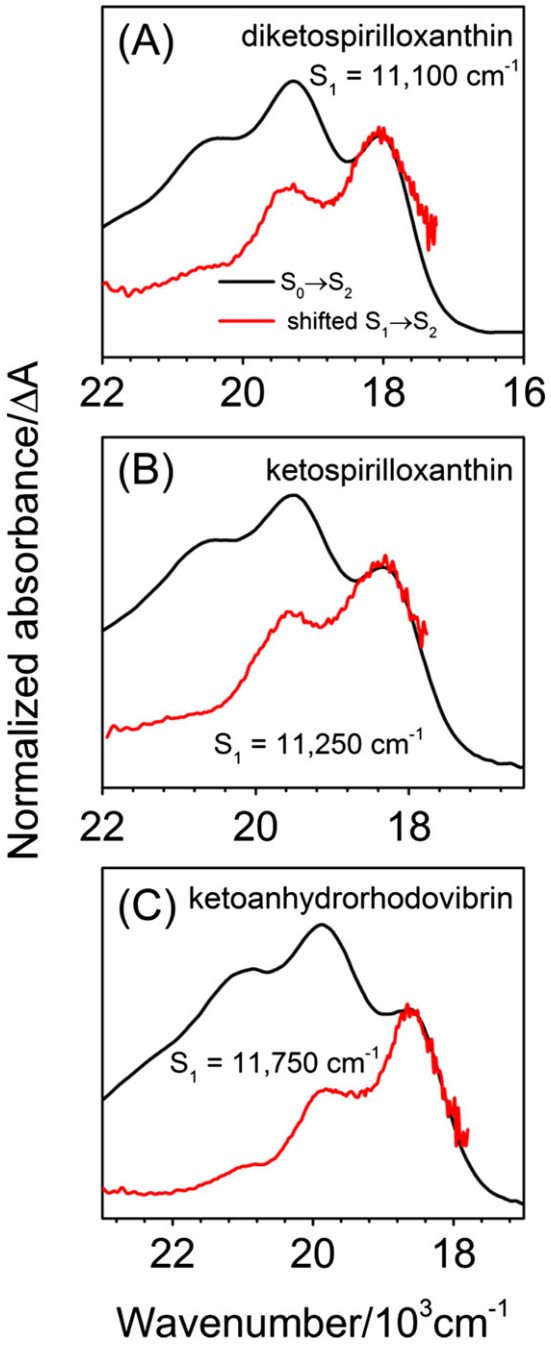

Fig. 6. The S_1 ($2^1A_g^-$) → S_2 ($1^1B_u^+$) excited-state absorption (red line) from NIR TA data at a pump–probe delay time at which S_2 ($1^1B_u^+$) → S_n ESA contributes negligibly, and energetically shifted for best coincidence with the S_0 ($1^1A_g^-$) → S_2 ($1^1B_u^+$) absorption profile (black line) from the steady-state absorption spectrum, for (A) diketospirilloxanthin, (B) ketospirilloxanthin and (C) ketoanhydrorhodovibrin in *n*-hex at RT. The magnitude of the spectral shift in each case determines the energy of S_1 ($2^1A_g^-$) state to be 11,100 cm^{-1} for diketospirilloxanthin, 11,250 cm^{-1} for ketospirilloxanthin and 11,750 cm^{-1} for ketoanhydrorhodovibrin.

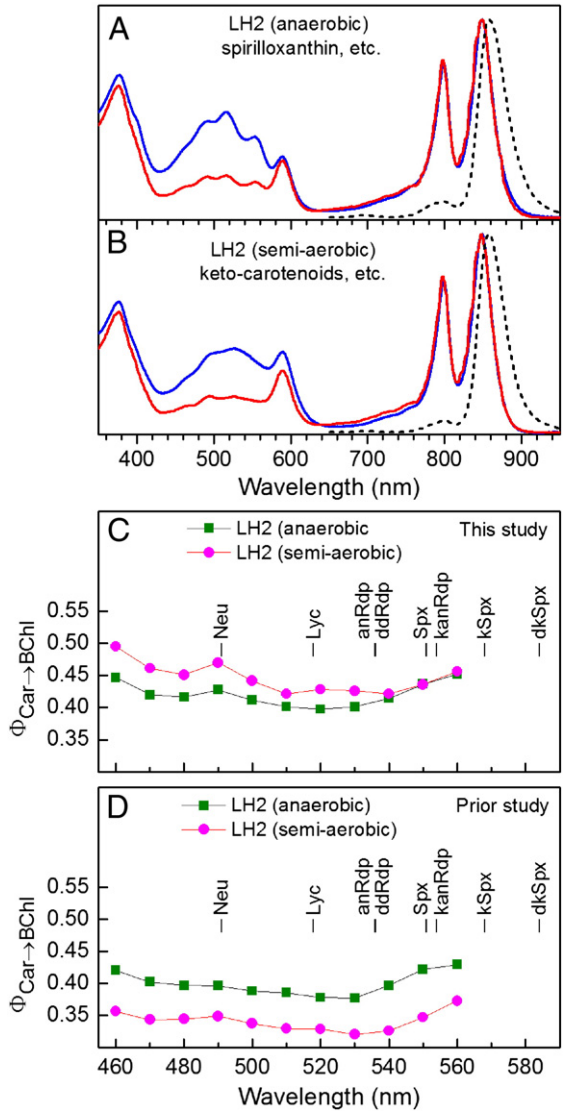

Fig. 7. Absorptance (1 − T) spectra (red) versus fluorescence excitation spectra (λ_{det} = 850 nm; blue), and B850 fluorescence spectra (λ_{exc} = 590 nm; dashed black) for LH2 studied here from *Rba. sphaeroides crtI::crtI*^{Pa} grown anaerobically (A) and semi-aerobically (B). Panel C shows wavelength-by-wavelength calculation of the $\Phi_{Car \rightarrow BChl}$ from the ratio of fluorescence-excitation versus absorptance amplitudes from the data in panel A (green symbols and line) and panel B (magenta symbols and line). The data in Panel D shows similar calculations of the energy-transfer efficiency for same *Rba. sphaeroides crtI::crtI*^{Pa} from different growth batches (length of time in light, etc.) and carotenoid contents from ref [17].

strain grown semi-aerobically. The fluorescence spectra (dashed black) were obtained using excitation of the BChls at 590 nm; spectra with the same shapes (but different amplitudes) were obtained at other excitation wavelengths, including exciting the carotenoid(s) in the 450–580 nm range. Fluorescence-excitation spectra (red) were obtained by monitoring the emission from the B850 BChls at 850 nm and scanning the excitation wavelengths between 350 and 1000 nm. The fluorescence-excitation spectra and absorptance (1 − T, where T is transmittance) spectra (blue) were normalized at 850 nm.

Fig. 7C shows the value of $\Phi_{Car \rightarrow BChl}$ obtained by measuring the amplitude ratio of the fluorescence-excitation versus absorptance spectra ratio as a function of wavelength across the carotenoid absorption region. The figure also shows the (0,0) positions of the carotenoids that contribute substantially to the content of one or both of the LH2 complexes (from strains grown anaerobically or semi-aerobically). As shown in Fig. 2C and D for each carotenoid, relative to the (0,0) band the absorption-contour maximum at the (1,0) band is tens of nanometers to shorter wavelengths and the entire contour spans over 100 nm to shorter wavelengths. Thus the various carotenoids present (Table 1) contribute broadly across the region shown in Fig. 7C.

Examination of the spectral reconstructions for the two LH2 samples (Fig. 2C and D) indicates that 540 nm is a reasonable compromise wavelength to obtain a yield value that has the least contributions from (1) shorter carotenoids ($N < 13$) that may be present (Table 1) and absorb at shorter wavelengths, and (2) direct excitation of B800 and B850 BChls in their Q_x band that peaks to longer wavelengths (~590 nm). A

contribution of either such species may shift the average $\Phi_{Car \rightarrow BChl}$ measured by excitation of a pigment mixture at a given wavelength to values larger than may be correct for individual or mixtures of carotenoid with $N = 13$–15. For example, the small increase in apparent $\Phi_{Car \rightarrow BChl}$ in progressing from 540 to 550 to 560 nm in Fig. 7C may arise from a contribution from (direct excitation in) the short-wavelength tail of the BChl Q_x band. Nonetheless, the data in Fig. 7C suggests that the $\Phi_{Car \rightarrow BChl}$ at 540 nm will give a good average for the key contributing carotenoids.

In this way, $\Phi_{Car \rightarrow BChl} = 0.41$ was determined for the LH2 from the *Rba. sphaeroides crtI::crtI*^{Pa} strain grown photosynthetically and basically the same value (0.42) was found for LH2 from the same strain semi-aerobically. Assessing these values in terms of the contributing carotenoids can be placed in a larger context by drawing up the analogous data shown in Fig. 7D. Those data were obtained from the earlier study of LH2 complexes derived from the same *Rba. sphaeroides* strain but using different growth batches (and purification protocols) and thus possessing different proportions of carotenoids.

The curves for $\Phi_{Car \rightarrow BChl}$ versus excitation wavelength for LH2 from the anaerobically strain studied here (Fig. 7C) are quite similar to those from the prior study (Fig. 7D), although perhaps shifted to slightly higher average values (e.g., 0.41 versus 0.40 at 540 nm and 0.40 versus 0.39 on the average at shorter wavelengths). Such a difference (if real) could be accounted for by the slightly lower (60%) spirilloxanthin ($N = 13$) in the sample studied here (Table 1) [along with 15% anhydrorhodovibrin ($N = 12$) and 8% lycopene ($N = 11$)] compared to (70%) spirilloxanthin in the sample studied previously [along with 13% anhydrorhodovibrin and 9% lycopene] [17].

The $\Phi_{Car \rightarrow BChl}$ levels are somewhat more different for LH2 obtained from the *Rba. sphaeroides crtI::crtI*^{Pa} strain grown semi-aerobically and studied here compared to that studied previously. In particular the $\Phi_{Car \rightarrow BChl}$ value using 540 nm excitation obtained here (0.42, Fig. 7C) is greater than the value from the prior study [17] (0.33, Fig. 7D). The average values encompassing shorter-wavelength excitation are 0.44 versus 0.35. Such modest differences are consistent with the altered ratios of the three key keto-bearing carotenoids ($N = 13$–15) and shorter ($N < 13$) carotenoids. In particular, the LH2 complexes isolated previously from semi-aerobically grown cells had 62% diketospirilloxanthin ($N = 13$), 16% ketospirilloxanthin ($N = 14$) and 14% ketoanhydrorhodovibrin ($N = 13$) and only very small amounts of shorter carotenoids such as anhydrorhodovibrin ($N = 12$) or lycopene ($N = 11$) [17]. The LH2 used for the present work had respectively 28%, 16% and 21% of the three keto-bearing carotenoids along with somewhat larger amounts of anhydrorhodovibrin (7%), didehydrorhodovibrin (6%) and lycopene (15%). The small amounts of these $N = 11$–12 carotenoids (and ratios of keto-bearing carotenoids) can easily account for the small increase in mean energy-transfer yield (0.44 versus 0.35) between the two samples when integrating over the entire absorption contour. Such a difference is truly modest when placed in the overall landscape of $\Phi_{Car \rightarrow BChl}$ values in LH2 complexes, including >90% typical for $N \leq 11$ carotenoids (Table 2) as noted in the Introduction and considered further below. The collective results speak to the low inherent $\Phi_{Car \rightarrow BChl}$ values for individual $N \geq 13$ carotenoids.

3.5.2. TA studies of energy flow in spirilloxanthin-containing LH2

Fig. 8 shows TA results for LH2 complexes from the photosynthetically grown *Rba. sphaeroides crtI::crtI*^{Pa} strain acquired at RT, and Figure S3 shows analogous data obtained at 77 K. This LH2 contains spirilloxanthin (60%) as the primary carotenoid, along with a lesser amount of anhydrorhodovibrin (15%) and still smaller amounts of shorter carotenoids (Table 1). The excitation wavelength (550 or 555 nm) was chosen to selectively excite spirilloxanthin, and no signals that can be easily associated with anhydrorhodovibrin are observed. In Fig. 8, the left panels are for the VIS region and the right panels for the NIR. The top panels give TA spectra at representative times, the middle

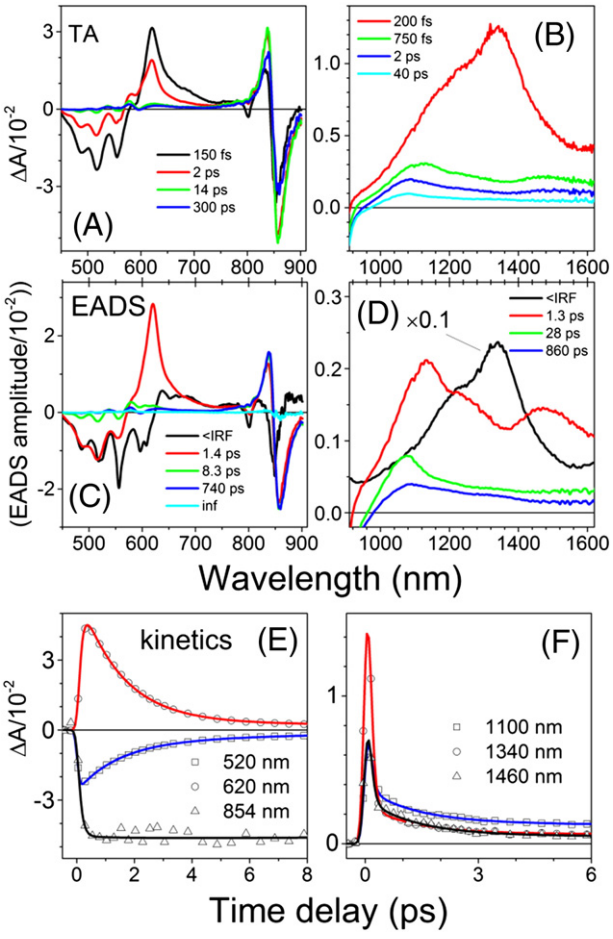

Fig. 8. Transient absorption results for LH2 from *Rba. sphaeroides crtI::crtI*^{Pa} grown anaerobically and containing primarily spirilloxanthin acquired at RT in the VIS (left panels) and NIR (right panels) using excitation at 555 nm. (A, B) Representative TA spectra. (C, D) Results of global analysis (EADS). (E) Representative kinetic profiles for decay of GSB (520 nm) and the decay of the S_1 ($2^1A_g^-$) state of spirilloxanthin probed at the maximum of the S_1 ($2^1A_g^-$) → S_n ESA band (620 nm) and the initial rise of the bleaching and slow recovery of the B850 excited state. (F) Representative kinetic profiles for decay of the S_2 ($1^1B_u^+$) and S_1 ($2^1A_g^-$) states probed at 1180 and 1515 nm. For panels (E) and (F), the data (symbols) are accompanied by fits using time constants obtained from global analysis (solid lines).

panels give the results of global analysis (EADS) and the bottom panels representative kinetic profiles and fits.

The spectra at the earliest times and the associated first EADS, which evolves within the instrument response function (~150 fs VIS, ~200 fs NIR), has characteristics expected for the S_2 ($2^1A_g^-$) state of spirilloxanthin and its decay and include GSB for the carotenoid absorption profile in the VIS and $S_2(1^1B_u^+) \rightarrow S_n$ absorption in the VIS and NIR. This EADS also shows simultaneous bleaching of both the B800 and B850 bands and a contribution of ESA in the VIS and NIR from the excited states of these BChl *a* species (B800* and B850*). The finding of BChl-associated features at these earliest times reflects ultrafast (<150 fs) energy transfer from the $S_2(1^1B_u^+)$ state of spirilloxanthin to both BChl *a* classes. The spirilloxanthin-to-BChl energy-transfer process may be less efficient at 77 K than at RT: the bleachings of the B800 and B850 bands are substantially smaller in relation to GSB of spirilloxanthin observed at RT. This effect is most likely associated with reduced energy transfer from the $S_2(1^1B_u^+)$ state due to reduced spectral overlap of fluorescence from the carotenoid $S_2(1^1B_u^+)$ state and the BChl Q_x absorption as the bands narrow at low temperature. Once energy arrives at B800, the 800-nm bleaching persists for a couple of picoseconds and then

disappears as B800* → B850 energy transfer occurs, in concert with direct transfer from the carotenoid $S_2(1^1B_u^+)$ to B850.

The spirilloxanthin $S_1(2^1A_g^-)$ excited state and its decay apparently primarily underpin the second EADS (red spectra in Fig. 8C and D). This assessment based on the similarity of the spectral shape to that obtained for the isolated carotenoid in various solvents and at various temperatures [35,39,41–45]. This includes a sharp positive $S_1(2^1A_g^-) \rightarrow S_n$ ESA band at 620 nm at RT at 624 nm at 77 K. The state decays with a time constant at RT of 1.4 ps (squares and blue curve for decay of GSB and circles and red curve for decay of $S_1(2^1A_g^-) \rightarrow S_n$ ESA in Fig. 8E). The lifetime of 1.4 ps is practically identical to values obtained from prior TA studies of spirilloxanthin in solution. This finding shows that the $S_1(2^1A_g^-)$ state is not involved in energy transfer to the B800 or B850 BChl *a* [35,39,41–45]. The $S_1(2^1A_g^-)$ lifetime lengthens slightly to 1.6 ps at 77 K (Figure S3), as observed previously for spirilloxanthin in solution [35,42].

The 8.3 ps EADS seen in the VIS (Fig. 8B) has some characteristics resembling those of the so-called carotenoid S* state (vide supra). It has been suggested that the S* state has properties that differ in LH2 versus organic media and is a precursor of the carotenoid triplet state [8,39,46,47]. The 28 ps EADS in the NIR data set that does not contribute significantly in the VIS may reflect decay of the spirilloxanthin radical cation formed in low yield via carotenoid–B800(BChl) interactions, as reported for numerous LH2 complexes [8,48,49].

The spectral shape of the EADS with an ~800 ps time evolution at RT [740 ps in VIS (Fig. 8C) and 860 ps in NIR (Fig. 8D)] is related to decay of B850*, the lowest singlet excited state of the excitonically coupled BChls. The B850* lifetime at 77 K lengthens to ~1100 ps (1140 ps in VIS and 1050 ps in NIR; Figure S3). In addition, the profile for B850 ground-state bleaching plus B850* stimulated emission is broader at 77 K than at RT. This effect may arise from a larger absorption–emission Stokes shift at low temperature, giving less overlap of the two contributions than at RT.

The longest "infinite" EADS (Fig. 8D) has a very small amplitude but has ESA characteristics expected for the spirilloxanthin triplet excited state. This state in LH2 is thought to formed via direct quenching of BChl *a* triplets and/or via spontaneous singlet excited state fission, presumably involving the S* state [6].

3.5.3. TA studies of energy flow in LH2 housing long-chain keto-bearing carotenoids

Fig. 9 shows RT TA results for the LH2 from the semi-aerobically grown *Rba. sphaeroides crtI::crtI*^{Pa}. Analogous data at 77 K are shown in Figure S4. This LH2 houses three long-chain carotenoids: diketospirilloxanthin (N = 15, 21%), ketospirilloxanthin (N = 14, 16%), ketoanhydrorhodovibrin (N = 13, 28%) along with lower N-value carotenoids including anhydrorhodovibrin (Table 1). The 542 nm excitation wavelength will excite all of these carotenoids to some extent, as indicated from the absorption spectral reconstruction (Fig. 2D). Thus, it might be expected that this LH2 shows more complex kinetic behavior than for LH2 containing a single or predominant carotenoid. However, apparently the spectral and temporal overlap of the features associated with the $S_1(2^1A_g^-)$ state of the three keto-bearing carotenoids blend into average characteristics.

The raw spectra and EADS in Figs. 9 and S4 show features analogous to those described above for the LH2 from the same strain grown anaerobically and containing primarily spirilloxanthin (Figs. 8 and S3). The features are associated with the GSB and ESA of carotenoids and with bleaching of the B800 and B850 bands. The evolution of the carotenoid S_2 $(1^1B_u^+)$ dominates the spectral and time evolution during the IRF, including rapid energy flow to the B800 and B850 BChl *a* species. The EADS with a 1.1–1.2 ps time evolution shows a broad carotenoid GSB profile that does not match the ground-state profile of any individual carotenoid. The spectrum also contains a somewhat broad ESA feature near 650 nm (Fig. 9C, red) that remains broad at 77 K although the time constant increases to 1.8 ps (Figure S4). This EADS likely reflects

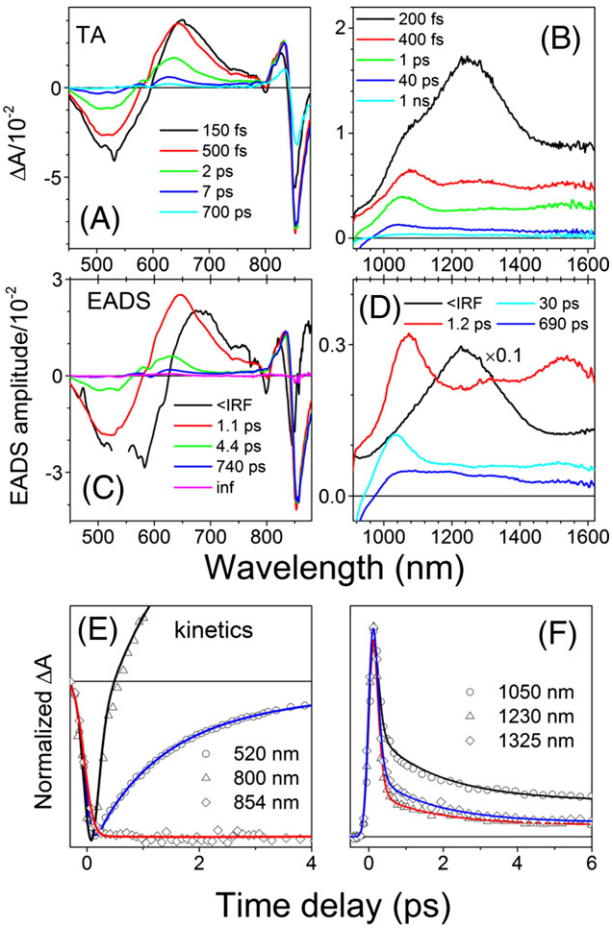

Fig. 9. Transient absorption results for LH2 from *Rba. sphaeroides crtI::crtI*^{Pa} grown semi-aerobically and containing a mixture of three long-chain keto-bearing carotenoids including diketospirilloxanthin acquired at RT in the VIS (left panels) and NIR (right panels) using excitation at 542 nm. (A, B) Representative TA spectra. (C, D) Results of global analysis (EADS). (E) Representative dynamics of the recovery of GSB (520 nm), dynamics of the initial rise and fast recovery of the B800 absorption band, and the rise of bleaching of the B850 exciton absorption. (F) Representative kinetic profiles for decay of the S_2 $(1^1B_u^+)$ and S_1 $(2^1A_g^-)$ states probed at various wavelengths. For panels (E) and (F), the data (symbols) are accompanied by fits using time constants obtained from global analysis (solid lines).

the combined $S_1(2^1A_g^-)$ excited states two or all three of keto-bearing (diketospirilloxanthin, ketospirilloxanthin, ketoanhydrorhodovibrin) and the observed time constant is an average $S_1(2^1A_g^-)$ lifetime (1.2 ps at RT, 1.8 ps at 77 K).

The next EADS observed at RT with a 4.4 ps lifetime has a much smaller amplitude than the 1.1 ps EADS (green versus red spectra in Fig. 9C), and is absent at 77 K when the excitation wavelength is shifted from 542 to 560 nm. The shape of this minor EADS resembles the vibronic bands at 535 and 500 nm expected for anhydrorhodovibrin/didehydrorhodopin (Fig. 2D). A lifetime 4.4 ps corresponds well to the $S_1(2^1A_g^-)$ lifetime of anhydrorhodovibrin measured in organic media [35].

The kinetic traces for decay of bleaching of carotenoid, B800 and B850 ground-state absorption bands (normalized at the t = 0 amplitude) are given in Fig. 9E. It is clear that the decay of the $S_1(2^1A_g^-)$ state(s) of the contributing long-chain keto-bearing carotenoids (circles and blue-line fit at 520 nm) does not induce additional bleaching of the B850 band (triangles and red-line fit at 854 nm). The rise of the B850 bleaching is coupled to decay of the B800 band (triangles and black-line fit) as energy flows rapidly from B800* to B850. Thus, by analogy with the LH2 that contains spirilloxanthin (N = 13) the $S_1(2^1A_g^-)$ state of keto-bearing carotenoids [ketoanhydrorhodovibrin (N = 13),

ketospirilloxanthin ($N = 14$) and diketospirilloxanthin ($N = 15$)] does not participate in energy transfer to the BChl *a* molecules.

Once formed via energy transfer from carotenoid $S_2(1^1B_u^+)$ and B800*, the B850* state of the excitonically coupled BChls in LH2 from semi-aerobically grown *Rba. sphaeroides crtI::crtI*^{Pa} decays with a time constant at RT of ~720 ps [740 ps VIS (Fig. 9C) and 690 ps NIR (Fig. 9D)], lengthening to 1.3 ps at 77 K (Figure S4). The decay time at both temperatures is comparable to that found above for the LH2 from semi-aerobically grown *Rba. sphaeroides crtI::crtI*^{Pa} that contains primarily spirilloxanthin (Figs. 8 and S3).

3.5.4. The $S_1(2^1A_g^-)$ energy of spirilloxanthin and long-chain keto-bearing carotenoids in LH2

The TA data presented herein for the LH2 complexes from the *Rba. sphaeroides crtI::crtI*^{Pa} strain grown anaerobically, which contains primarily spirilloxanthin ($N = 13$) and grown semi-aerobically, which contains a mixture of keto-bearing long-chain analogues [ketoanhydrorhodovibrin ($N = 13$), ketospirilloxanthin ($N = 14$) and diketospirilloxanthin ($N = 15$)], affords a means to estimate the energy of the $S_1(2^1A_g^-)$ states of these carotenoids and compare with the results for the isolated carotenoids in organic media. A prior such comparison showed that the $S_1(2^1A_g^-)$ energy for spirilloxanthin in LH1 is the same as in solution [41], and thus that the protein environment does not alter the structural/electronic characteristics of this carotenoid. However, such a comparison has not been made for spirilloxanthin in LH2, or for the long-chain keto-bearing carotenoids.

The energy of the $S_1(2^1A_g^-)$ state for LH2-bound carotenoids for *Rba. sphaeroides crtI::crtI*^{Pa} strain grown anaerobically and semi-aerobically was calculated from spectroscopic data using the same methodology described above for isolated diketospirilloxanthin, ketospirilloxanthin and ketoanhydrorhodovibrin in *n*-hex at RT (Fig. 6) and diketospirilloxanthin at 77 K (Figure S2). The results are presented in Fig. 10.

Before spectral matching, the NIR TA spectrum with the $S_1(2^1A_g^-) \rightarrow S_2(1^1B_u^+)$ ESA band present was corrected for overlap with the ESA band of the long-lived B850* excited state. The latter was taken from the TA spectrum recorded at later delay times, after complete decay of the carotenoid $S_1(2^1A_g^-)$ state. The resulting corrected $S_1(2^1A_g^-) \rightarrow S_2(1^1B_u^+)$ ESA profiles are the red traces in Fig. 10. The solid black traces are the observed $S_0\ (1^1A_g^-) \rightarrow S_2\ (1^1B_u^+)$ steady-state absorption profiles of the LH2, which includes contributions from all carotenoids present as well as the Q_x absorption band of the B800 and B850 BChls (~17,000 cm^{-1}). The dashed black spectrum in Fig. 10A is the steady-state absorption of spirilloxanthin obtained from spectral reconstruction of the carotenoid contour in that LH2 (anaerobic growth) (Fig. 2C). The dashed spectrum in Fig. 10B reflects a mixture of the steady-state absorption spectra diketospirilloxanthin, ketospirilloxanthin and ketoanhydrorhodovibrin (Fig. 2D) with proportions given by their percent contribution (Table 1) to the total carotenoid content of that LH2 (semi-anaerobic growth). In both cases, the carotenoid contour chosen should reflect the major carotenoids elevated to the excited state by the excitation flash in the TA experiments that afford the $S_1(2^1A_g^-) \rightarrow S_2(1^1B_u^+)$ ESA profile. Because of the mixture in the semi-aerobically grown strain, there is necessarily some uncertainty in matching the $S_1(2^1A_g^-) \rightarrow S_2(1^1B_u^+)$ ESA (red) and $S_0(1^1A_g^-) \rightarrow S_2(1^1B_u^+)$ vibronic contours to obtain the $S_0(1^1A_g^-)$ energy. Additionally the higher-energy side of the ESA profile may be enhanced by absorption of carotenoid cation present on the same time scale as the $S_1(2^1A_g^-)$ state, resulting in poor alignment on the higher energy portion of the contours. Although these factors may affect the precise $S_1(2^1A_g^-)$ energies derived, they do not compromise the overall conclusions.

The derived $S_1(2^1A_g^-)$ state energy of 11,300 cm^{-1} for spirilloxanthin in LH2 (Fig. 10A) is practically the same as in organic solvents (Table 2); thus the effective conjugation length is not affected by protein binding pocket. The derived $S_1(2^1A_g^-)$ state energy of

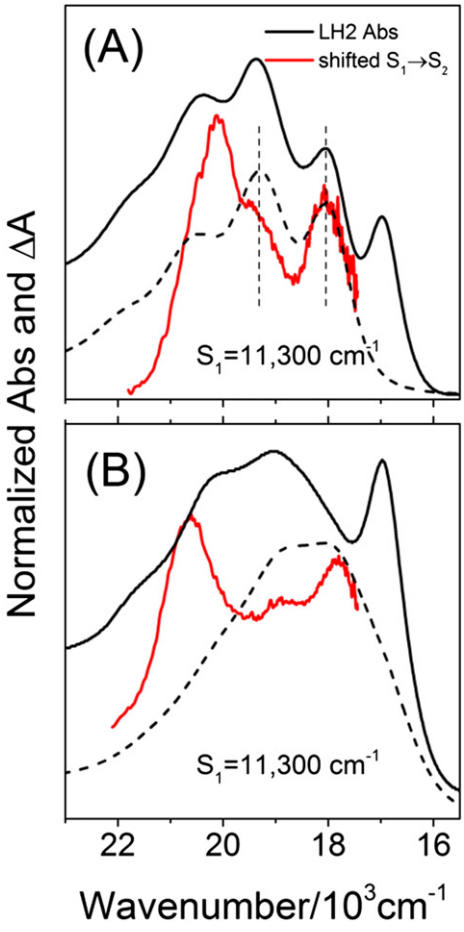

Fig. 10. Analysis of the $S_1\ (2^1A_g^-)$ energy from data acquired at RT for LH2 complexes from *Rba. sphaeroides crtI::crtI*^{Pa} grown anaerobically (A) and containing primarily spirilloxanthin, and grown semi-aerobically and containing a mixture of diketospirilloxanthin, ketospirilloxanthin and ketoanhydrorhodovibrin (B). The solid black spectrum in each panel is the observed steady-state $[S_0\ (1^1A_g^-) \rightarrow S_2\ (1^1B_u^+)]$ absorption spectrum. The $S_1\ (2^1A_g^-) \rightarrow S_2\ (1^1B_u^+)$ TA spectra (red) were extracted from the NIR TA datasets at delay times at which contribution from the $S_2\ (1^1B_u^+) \rightarrow S_n$ ESA is negligible and shifted in energy to give best coincidence with steady-state absorption of the contributing carotenoid(s) in that LH2 (dashed lines). The latter utilized the spectra obtained from the spectral reconstructions in Fig. 2C and D. For panel A, the dashed spectrum is that for spirilloxanthin, the predominant carotenoid. For panel B, the dashed spectrum reflects a mixture of diketospirilloxanthin, ketospirilloxanthin and ketoanhydrorhodovibrin in proportion to percentage of the LH2 content (Table 1). The magnitude of the energy shift of the TA spectra determines the energy of the $S_1\ (2^1A_g^-)$ state of the carotenoids.

11,300 cm^{-1} for the mixture of diketospirilloxanthin, ketospirilloxanthin and ketoanhydrorhodovibrin in LH2 (Fig. 10B) is comparable to the average value for the three keto-bearing carotenoids in *n*-hex (Fig. 6). The implications of these findings for the functional characteristics of these carotenoids in the LH2 antennas are given in the Discussion section.

4. Discussion

The rates, efficiencies and mechanisms of Car → BChl energy transfer in LH2 complexes from a variety of bacterial species have been studied extensively by static and time-resolved absorption spectroscopy, as noted in the Introduction. The carotenoid content of LH2 was varied by choice of bacterial strain, growth conditions and reconstitution into carotenoid-free LH2 complexes. Such studies have primarily involved LH2 containing carotenoids with conjugation lengths up to $N = 11$, for which spheroidenone ($N_{C=C} = 10$, $N_{C=O} = 1$) is the prime keto-bearing example. The photophysical properties of such carotenoids

(including spirilloxanthin, $N = 13$) also have been studied in organic solvents with a range of polarities and polarizabilities at RT and 77 K [8,35,50–52]. Table 2 collects the excited-state lifetimes and energies from some of the prior work, along with the data obtained herein. The present results on spirilloxanthin ($N = 13$) and long-chain keto-bearing carotenoids ketoanhydrorhodovibrin, ketospirilloxanthin and diketospirilloxanthin ($N = 12$–15) in LH2 and organic media add to the large body of prior work by many groups. Key findings and comparisons are highlighted in the following.

The recent study by Chi et al. [17] introduced a series of genetically engineered *Rba. sphaeroides* strains that produce LH2 (and LH1) housing carotenoids from $N = 9$ to 15. The LH2 from some strains contain primarily one carotenoid while others afford mixtures with ratios that depend on growth conditions. This is not surprising for purple sulfur bacteria that employ the spirilloxanthin biosynthesis pathway. The LH2 sample studied here from *Rba. sphaeroides crtI::crtI*^{Pa} grown anaerobically contains 60% spirilloxanthin (Table 1), which is similar to the 70% obtained for a different growth batch from the initial study [12]. In both studies, $\Phi_{Car \rightarrow BChl} \sim 0.4$ is found when the excitation light is absorbed predominantly by spirilloxanthin or in part by other carotenoids present (Fig. 6). The LH2 sample studied here from *Rba. sphaeroides crtI::crtI*^{Pa} grown semi-aerobically contains a mixture of ketoanhydrorhodovibrin, ketospirilloxanthin and diketospirilloxanthin (Table 1) whereas LH2 from the prior study had 60% diketospirilloxanthin. Nonetheless, $\Phi_{Car \rightarrow BChl}$ in the range ~0.35 to ~0.45 is found with differences consistent with the measured carotenoid ratios.

These results show that that $\Phi_{Car \rightarrow BChl}$ is ~0.4 (or slightly lower) for $N = 13$ carotenoids anhydrorhodovibrin ($N_{C=C} = 12$, $N_{C=O} = 1$) and spirilloxanthin ($N_{C=C} = 13$, $N_{C=O} = 0$) and upon extension via incorporation of the terminal keto groups in ketospirilloxanthin ($N_{C=C} = 13$, $N_{C=O} = 1$) and diketospirilloxanthin ($N_{C=C} = 13$, $N_{C=O} = 2$). It is also found that the lifetime of the $S_1(2^1A_g^-)$ excited state of spirilloxanthin in the anaerobically grown *Rba. sphaeroides crtI::crtI*^{Pa} and the average $S_1(2^1A_g^-)$ lifetime of the trio of keto-bearing long chain analogs in the semi-aerobically grown strain are similar to the values for the isolated carotenoids in organic media. The combined results suggest that the $S_1(2^1A_g^-)$ excited state of the $N \geq 13$ carotenoids participates little if at all in energy transfer to the B800 or B850 BChls. This conclusion supports the hypothesis from studies of carotenoids up to $N = 11$ that only carotenoids with $N \leq 10$ transfer energy via their $S_1(2^1A_g^-)$ states to BChl *a* in LH2 to any significant degree [53].

The finding of modestly greater $\Phi_{Car \rightarrow BChl}$ of ~0.5 to ~ 0.65 for $N = 11$ carotenoids (e.g., lycopene, rhodopin, rhodopin glucoside) [8,12,13,54] would then be consistent with the $S_1(2^1A_g^-)$ pathway remaining partially active or that the yield (and rate constant) of the $S_2(1^1B_u^+)$ pathway increases modestly as N decreases, and by extension contributing modestly more than the $S_1(2^1A_g^-)$ pathway for the $N = 9$–11 carotenoids in LH2 antennas. The present results also bear on the finding that $N = 11$ spheroidenone ($N_{C=C} = 10$, $N_{C=O} = 1$) has the high $\Phi_{Car \rightarrow BChl}$ (0.90–0.95) of the shorter carotenoids ($N = N_{C=C} = 9$–10). In this molecule the normal $S_1(2^1A_g^-)$ and $S_2(1^1B_u^+)$ pathways may be augmented by participation of keto-associated excited states such as intramolecular charge-transfer (ICT) state [55] which is not formed in longer-chain ($N \geq 11$) keto-bearing carotenoids as studied here: ketoanhydrorhodovibrin, ketospirilloxanthin and diketospirilloxanthin. It has also been suggested that change in symmetry engendered by addition of a keto group enhances the efficiency of energy transfer via the $S_1(2^1A_g^-)$ pathway [56]. Regardless, such mechanisms do not provide such enhancements for the longer-chain keto-bearing carotenoids.

The simplest, unifying explanation for all the above-noted observations is if the $S_1(2^1A_g^-)$ state for the $N \geq 13$ carotenoids (with or without keto groups) has dropped energetically near or below the B850* excited state of the excitonically coupled BChl *a* array, and thus energy transfer is ineffective on energetic grounds. This question was addressed here via TA studies to determine the energies of $S_1(2^1A_g^-)$ and $S_2(1^1B_u^+)$ excited states of these carotenoids in LH2 complexes from *Rba. sphaeroides crtI::crtI*^{Pa} (grown anaerobically or semi-aerobically) and isolated in organic media. As noted above, prior studies have provided such information for numerous carotenoids without keto groups and for the keto-bearing spheroidenone ($N = 11$). The results are listed in Table 2 and shown graphically in Fig. 11. Notable findings are as follows.

(1) The energy of the $S_1(2^1A_g^-)$ state for $N \geq 13$ carotenoids (e.g., spirilloxanthin, ketospirilloxanthin, diketospirilloxanthin) measured in *n*-hex at RT is close to or below that for B850* (11,780 cm^{-1}, black dotted line in Fig. 11A). The same holds for these carotenoids when bound in LH2. As noted above, the $S_1(2^1A_g^-)$ energy for spirilloxanthin in LH2 is the same in LH2 (anaerobically grown *Rba. sphaeroides crtI::crtI*^{Pa}) as in organic

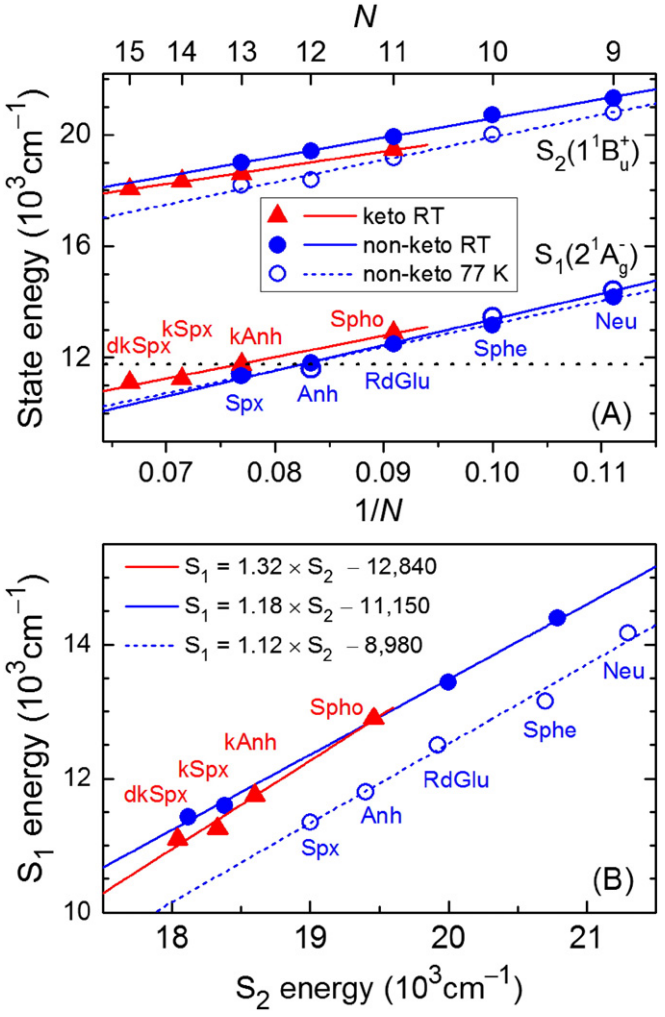

Fig. 11. (A) The S_1 ($2^1A_g^-$) and S_2 ($1^1B_u^+$) state energies of two classes of open chain carotenoids found in LH2 complexes from either sulfur on non-sulfur purple bacteria: non-keto carotenoids (blue circles) [neurosporene (Neu), spheroidene (Sphe), rhodopin glucoside (RdGlu), anhydrorhodovibrin (Anh), spirilloxanthin (Spx)], and keto-bearing carotenoids (red triangles) [spheroidenone (Spho), ketospirilloxanthin (kSpx), ketoanhydrorhodovibrin (kAnh), diketospirilloxanthin (dkSpx)] obtained at RT (closed symbols and solid lines) and at 77 K (open symbols and dashed lines) as a function of the total number of conjugated double bonds (N). The energies of the S_2 ($1^1B_u^+$) state originate from steady-state absorption spectra taken in *n*-hex (except for rhodopin glucoside that was measured in methanol) while the energies of the S_1 ($2^1A_g^-$) state are obtained from measuring the S_1–S_2 energy gap by transient absorption in various solvents (see Table 2 for details). The dotted black horizontal line in (A) is the energy of the B850* excited state of the BChl *a* array in LH2 at RT. (B) The S_1 ($2^1A_g^-$) state energy as a function of the S_2 ($1^1B_u^+$) state energy. The data were fit with linear functions having equations given in the graph.

media, and the average value for ketoanhydrorhodovibrin, ketospirilloxanthin, diketospirilloxanthin (semi-aerobically grown *Rba. sphaeroides crtI::crtI*^{Pa}) is comparable to the average for the three individual carotenoids in *n*-hex at RT.

(2) Freezing the medium at cryogenic temperature has relatively small impact on the $S_1(2^1A_g^-)$ state energy of the non-keto open-chain carotenoids.

(3) As expected based on prior work, the large polarizability of the 2-MTHF glass at cryogenic temperature downshifts the energy of $S_2(1^1B_u^+)$ for the non-keto carotenoids. However, the trend lines for the state energy versus 1/*N* at RT (*n*-hex) and 77 K (2-MTHF) are not parallel and temperature-induced energetic shift becomes larger as *N* increases, as exemplified by the points for neurosporene and spirilloxanthin in Fig. 11A. Perhaps in addition to the increased medium polarizability in 2-MTHF at 77 K, torsional motions involving the terminal regions of the longer chains are reduced in the frozen medium, thereby slightly increasing the effective conjugation with the carbon–carbon backbone.

(4) The trend-line for the $S_2(1^1B_u^+)$ energy versus 1/*N* (or *N*) for the keto-bearing carotenoids (solid red line) lies vertically below that for analogs that do not have a keto group (solid blue line), whereas the reverse is true for $S_1(2^1A_g^-)$. To obtain overlap, the trend-line for $S_2(1^1B_u^+)$ of keto-bearing carotenoids (red) must be shifted (left) along the 1/*N* (or *N*) by an amount corresponding to one additional C═C bond (blue), whereas the reverse is true for $S_1(2^1A_g^-)$. In other words, addition of one C═O bond decreases the $S_2(1^1B_u^+)$ energy by an amount that would be expected upon increasing *N* with two C═C bonds, while addition of a C═O bond has a relatively small effect on the S_1 $(2^1A_g^-)$ energy (about one less than addition of a C═C bond). Thus, depending on what is being probed, a C═O bond addition may appear to have anywhere between zero and twice the effect of a C═C bond. One view of these findings is that the carotenoids differ structurally in the two states, perhaps with different torsion angles between terminal C═O group(s) and the carbon–carbon backbone, such that in $S_2(1^1B_u^+)$ effective conjugation is longer than for $S_1(2^1A_g^-)$. Another view is that the electronic structures and excited-state manifolds of keto-bearing carotenoids differ sufficiently to warrant treatment as a distinct carotenoid class; thus, there is a risk of oversimplifying the relative effects of adding C═O or C═C bonds.

Finally, the analysis given above has been mainly focused on the effects of addition of C═C and especially C═O bonds to achieve nominal conjugation lengths *N* ranging from 13 to 15. It has been shown that the $S_1(2^1A_g^-)$ state energies for such carotenoids (ketoanhydrorhodovibrin, spirilloxanthin, ketospirilloxanthin and diketospirilloxanthin) lie energetically near or below the excited B850 ring of coupled BChls. Thus, direct quenching of B850* by the carotenoid is energetically favorable, especially in diketospirilloxanthin-containing LH2 (i.e., *Rba. sphaeroides crtI::crtI*^{Pa} grown semi-aerobically). Direct quenching of Chls by carotenoid via energy transfer has been reported previously in TA studies of isolated LHCII complexes from higher plants [57] and in IsiA complex [58], and HliD protein from cyanobacteria [59]. However, to our knowledge this effect has not been observed for an LH2 complex, likely due to the lack of LH2 antennas that contain substantial amounts of carotenoids with very long conjugation lengths.

A hint that carotenoid-mediated BChl *a* quenching in these LH2 complexes may occur is an apparent shortening of the B850* lifetime. In *Rba. sphaeroides crtI::crtI*^{Pa} grown anaerobically (containing primarily spirilloxanthin) and semi-aerobically (containing a mixture of keto-carotenoids including diketospirilloxanthin), the B850* lifetime at RT is ~0.8 ns. This value is modestly shorter than the value of ~1 ns or slightly longer than found previously for most LH2 complexes (with generally containing shorter carotenoids) [60–62]. However, assessing whether this difference reflects carotenoid quenching of B850* or arises from differences in the time-resolved measurements (e.g., excited-state annihilation) and/or LH2 samples (e.g., different extent of interactions between LH2 rings) must await studies of a unified set of LH2 complexes differing only in carotenoid conjugation length. The availability of *Rba. sphaeroides* mutants [17] that can produce LH2 (and LH1) complexes with such a diversity of carotenoids in a single organism will facilitate this endeavor and other comparisons of carotenoid functional properties in photosynthetic light-harvesting systems.

Transparency document

The Transparency document associated with this article can be found in the online version.

Acknowledgements

This research was performed as a part of the Photosynthetic Antenna Research Center, an Energy Frontier Research Center funded by the U.S. DOE, Office of Basic Energy Sciences (Grant No. DE-SC 0001035). That grant supported the growth and isolation of bacterial cells (U.K.) and the static/time-resolved spectroscopy on the LH2 complexes (U.S.). For generation of the mutant strain and initial characterization studies, C.N.H. and E.C.M. acknowledge financial support from the Biotechnology and Biological Sciences Research Council (UK) award numbers BB/G021546/1 and BB/M000265/1. C.N.H. was also supported by an Advanced Award 338895 from the European Research Council. D.J.M. was supported by a doctoral studentship from the Biotechnology and Biological Sciences Research Council (U.K.).

Appendix A. Supplementary data

Supplementary data to this article can be found online at http://dx.doi.org/10.1016/j.bbabio.2015.04.001.

References

[1] G. McDermott, S.M. Prince, A.A. Freer, A.M. Hawthornthwaite-Lawless, M.Z. Papiz, R.J. Cogdell, N.W. Isaacs, Crystal structure of an integral membrane light-harvesting complex from photosynthetic bacteria, Nature 374 (1995) 517–521.
[2] S.M. Prince, M.Z. Papiz, A.A. Freer, G. McDermott, A.M. Hawthornthwaite-Lawless, R.J. Cogdell, N.W. Isaacs, Apoprotein structure in the LH2 complex from *Rhodopseudomonas acidophila* strain 10050: modular assembly and protein pigment interactions, J. Mol. Biol. 268 (1997) 412–423.
[3] M.Z. Papiz, S.M. Prince, T. Howard, R.J. Cogdell, N.W. Isaacs, The structure and thermal motion of the B800–850 LH2 complex from *Rps. acidophila* at 2.0 Å resolution and 100 K: New structural features and functionally relevant motions, J. Mol. Biol. 326 (2003) 1523–1538.
[4] J. Koepke, X. Hu, C. Muenke, K. Schulten, H. Michel, The crystal structure of the light-harvesting complex II (B800-850) from *Rhodospirillum molischianum*, Structure 4 (1996) 581–597.
[5] N.I. Krinsky, Function, in: O. Isler, N. Guttman, U. Solms (Eds.), Carotenoids, Birghäuser Verlag, Basel, Switzerland 1971, p. 669.
[6] Y. Kakitani, J. Akahane, H. Ishii, H. Sogabe, H. Nagae, Y. Koyama, Conjugation-length dependence of the T_1 lifetimes of carotenoids free in solution and incorporated into the LH2, LH1, RC, and RC–LH1 complexes: possible mechanisms of triplet-energy dissipation, Biochemistry 46 (2007) 2181–2197.
[7] V. Šlouf, P. Chabera, J.D. Olsen, E.C. Martin, P. Qian, C.N. Hunter, T. Polivka, Photoprotection in a purple phototrophic bacterium mediated by oxygen-dependent alteration of carotenoid excited-state properties, Proc. Natl. Acad. Sci. U. S. A. 109 (2012) 8570–8575.
[8] H. Cong, D.M. Niedzwiedzki, G.N. Gibson, A.M. LaFountain, R.M. Kelsh, A.T. Gardiner, R.J. Cogdell, H.A. Frank, Ultrafast time-resolved carotenoid to-bacteriochlorophyll energy transfer in LH2 complexes from photosynthetic bacteria, J. Phys. Chem. B 112 (2008) 10689–10703.
[9] T. Polivka, H.A. Frank, Molecular factors controlling photosynthetic light harvesting by carotenoids, Acc. Chem. Res. 43 (2010) 1125–1134.
[10] A. Angerhofer, F. Bornhauser, A. Gall, R.J. Cogdell, Optical and optically detected magnetic-resonance investigation on purple photosynthetic bacterial antenna complexes, Chem. Phys. 194 (1995) 259–274.
[11] H.A. Frank, R.J. Cogdell, Carotenoids in photosynthesis, Photochem. Photobiol. 63 (1996) 257–264.

[12] G. Garcia-Asua, R.J. Cogdell, C.N. Hunter, Functional assembly of the foreign carotenoid lycopene into the photosynthetic apparatus of *Rhodobacter sphaeroides*, achieved by replacement of the native 3-step phytoene desaturase with its 4-step counterpart from *Erwinia herbicola*, Mol. Microbiol. 44 (2002) 233–244.
[13] H.H. Billsten, J.L. Herek, G. Garcia-Asua, L. Hashoj, T. Polivka, C.N. Hunter, V. Sundstrom, Dynamics of energy transfer from lycopene to bacteriochlorophyll in genetically-modified LH2 complexes of *Rhodobacter sphaeroides*, Biochemistry 41 (2002) 4127–4136.
[14] D.M. Niedzwiedzki, M. Kobayashi, R.E. Blankenship, Triplet excited state spectra and dynamics of carotenoids from the thermophilic purple photosynthetic bacterium *Thermochromatium tepidum*, Photosynth. Res. 107 (2011) 177–186.
[15] D.M. Niedzwiedzki, D. Bina, N. Picken, S. Honkanen, R.E. Blankenship, D. Holten, R.J. Cogdell, Spectroscopic studies of two spectral variants of light-harvesting complex 2 (LH2) from the photosynthetic purple sulfur bacterium *Allochromatium vinosum*, BBA-Bioenerg. 1817 (2012) 1576–1587.
[16] G. Garcia-Asua, H.P. Lang, R.J. Cogdell, C.N. Hunter, Carotenoid diversity: a modular role for the phytoene desaturase step, Trends Plant Sci. 3 (1998) 445–449.
[17] S.C. Chi, D.J. Mothersole, P. Dilbeck, D.M. Niedzwiedzki, H. Zhang, P. Qian, C. Vasilev, K.J. Grayson, P.J. Jackson, E.C. Martin, Y. Li, D. Holten, C.N. Hunter, Assembly of functional photosystem complexes in *Rhodobacter sphaeroides* incorporating carotenoids from the spirilloxanthin pathway, BBA-Bioenerg. 1847 (2014) 189–201.
[18] S. Kereiche, L. Bourinet, W. Keegstra, A.A. Arteni, J.M. Verbavatz, E.J. Boekema, B. Robert, A. Gall, The peripheral light-harvesting complexes from purple sulfur bacteria have different 'ring' sizes, FEBS Lett. 582 (2008) 3650–3656.
[19] A.M. Carey, K. Hacking, N. Picken, S. Honkanen, S. Kelly, D.M. Niedzwiedzki, R.E. Blankenship, Y. Shimizu, Z.Y. Wang-Otomo, R.J. Cogdell, Characterisation of the LH2 spectral variants produced by the photosynthetic purple sulphur bacterium *Allochromatium vinosum*, BBA-Bioenerg. 1837 (2014) 1849–1860.
[20] I.H. van Stokkum, D.S. Larsen, R. van Grondelle, Global and target analysis of time-resolved spectra, BBA-Bioenerg. 1657 (2004) 82–104.
[21] T. Gerjets, S. Steiger, G. Sandmann, Catalytic properties of the expressed acyclic carotenoid 2-ketolases from *Rhodobacter capsulatus* and *Rubrivivax gelatinosus*, BBA-Mol. Cell Biol. Lipids 1791 (2009) 125–131.
[22] P.C. Lee, E. Holtzapple, C. Schmidt-Dannert, Novel activity of *Rhodobacter sphaeroides* spheroidene monooxygenase CrtA expressed in *Escherichia coli*, Appl. Environ. Microbiol. 76 (2010) 7328–7331.
[23] G. Britton, S. Liaaen-Jensen, H. Pfander, Handbook, Carotenoids, Birkhäuser Basel, Basel, Boston, Berlin, 2004.
[24] A. Gall, R.J. Cogdell, B. Robert, Influence of carotenoid molecules on the structure of the bacteriochlorophyll binding site in peripheral light-harvesting proteins from *Rhodobacter sphaeroides*, Biochemistry 42 (2003) 7252–7258.
[25] L. Fiedor, J. Akahane, Y. Koyama, Carotenoid-induced cooperative formation of bacterial photosynthetic LH1 complex, Biochemistry 43 (2004) 16487–16496.
[26] C. Theiss, D. Leupold, A.A. Moskalenko, A.P. Razjivin, H.J. Eichler, H. Lokstein, Femtosecond spectroscopy of native and carotenoidless purple-bacterial LH2 clarifies functions of carotenoids, Biophys. J. 94 (2008) 4808–4811.
[27] J.C. Merlin, Resonance Raman-spectroscopy of carotenoids and carotenoid-containing systems, Pure Appl. Chem. 57 (1985) 785–792.
[28] Y. Koyama, I. Takatsuka, M. Nakata, M. Tasumi, Raman and infrared-spectra of the all-*trans*, 7-*cis*, 9-*cis*, 13-*cis* and 15-*cis* isomers of β-carotene — key bands distinguishing stretched or terminal-bent configurations from central-bent configurations, J. Raman Spectrosc. 19 (1988) 37–49.
[29] M.M. Mendes-Pinto, E. Sansiaume, H. Hashimoto, A.A. Pascal, A. Gall, B. Robert, Electronic absorption and ground state structure of carotenoid molecules, J. Phys. Chem. B 117 (2013) 11015–11021.
[30] R.L. Christensen, The electronic states of carotenoids, in: A.J. Frank, A.J. Young, D. Britton, J.W. Cogdell (Eds.), Photochemistry of Carotenoids, Kluwer Academic Publishers, Dordrecht, Boston, London 1999, pp. 137–159.
[31] J.P. Zhang, L.H. Skibsted, R. Fujii, Y. Koyama, Transient absorption from the $1B_u^+$ state of all-*trans*-β-carotene newly identified in the near-infrared region, Photochem. Photobiol. 73 (2001) 219–222.
[32] T. Polivka, V. Sundstrom, Ultrafast dynamics of carotenoid excited states—from solution to natural and artificial systems, Chem. Rev. 104 (2004) 2021–2071.
[33] T. Polivka, V. Sundstrom, Dark excited states of carotenoids: consensus and controversy, Chem. Phys. Lett. 477 (2009) 1–11.
[34] T. Polivka, D. Zigmantas, H.A. Frank, J.A. Bautista, J.L. Herek, Y. Koyama, R. Fujii, V. Sundstrom, Near-infrared time-resolved study of the S_1 state dynamics of the carotenoid spheroidene, J. Phys. Chem. B 105 (2001) 1072–1080.
[35] D. Niedzwiedzki, J.F. Koscielecki, H. Cong, J.O. Sullivan, G.N. Gibson, R.R. Birge, H.A. Frank, Ultrafast dynamics and excited state spectra of open-chain carotenoids at room and low temperatures, J. Phys. Chem. B 111 (2007) 5984–5998.
[36] D.M. Niedzwiedzki, M.M. Enriquez, A.M. LaFountain, H.A. Frank, Ultrafast time-resolved absorption spectroscopy of geometric isomers of xanthophylls, Chem. Phys. 373 (2010) 80–89.
[37] P.O. Andersson, T. Gillbro, Photophysics and dynamics of the lowest excited singlet state in long substituted polyenes with implications to the very long chain limit, J. Chem. Phys. 103 (1995) 2509–2519.
[38] W. Wohlleben, T. Buckup, H. Hashimoto, R.J. Cogdell, J.L. Herek, M. Motzkus, Pump–deplete–probe spectroscopy and the puzzle of carotenoid dark states, J. Phys. Chem. B 108 (2004) 3320–3325.
[39] C.C. Gradinaru, J.T. Kennis, E. Papagiannakis, I.H. van Stokkum, R.J. Cogdell, G.R. Fleming, R.A. Niederman, R. van Grondelle, An unusual pathway of excitation energy deactivation in carotenoids: singlet-to-triplet conversion on an ultrafast timescale in a photosynthetic antenna, Proc. Natl. Acad. Sci. U. S. A. 98 (2001) 2364–2369.
[40] D.M. Niedzwiedzki, J.O. Sullivan, T. Polivka, R.R. Birge, H.A. Frank, Femtosecond time-resolved transient absorption spectroscopy of xanthophylls, J. Phys. Chem. B 110 (2006) 22872–22885.
[41] E. Papagiannakis, I.H.M. van Stokkum, R. van Grondelle, R.A. Niederman, D. Zigmantas, V. Sundstrom, T. Polivka, A near-infrared transient absorption study of the excited-state dynamics of the carotenoid spirilloxanthin in solution and in the LH1 complex of *Rhodospirillum rubrum*, J. Phys. Chem. B 107 (2003) 11216–11223.
[42] D.M. Niedzwiedzki, D.J. Sandberg, H. Cong, M.N. Sandberg, G.N. Gibson, R.R. Birge, H.A. Frank, Ultrafast time-resolved absorption spectroscopy of geometric isomers of carotenoids, Chem. Phys. 357 (2009) 4–16.
[43] K. Nishimura, F.S. Rondonuwu, R. Fujii, J. Akahane, Y. Koyama, T. Kobayashi, Sequential singlet internal conversion of $1B_u^+ \rightarrow 3A_g^- \rightarrow 1B_u^- \rightarrow 2A_g^- \rightarrow 1A_g^-$ ground in all-*trans*-spirilloxanthin revealed by two-dimensional sub-5-fs spectroscopy, Chem. Phys. Lett. 392 (2004) 68–73.
[44] R. Fujii, T. Inaba, Y. Watanabe, Y. Koyama, J.P. Zhang, Two different pathways of internal conversion in carotenoids depending on the length of the conjugated chain, Chem. Phys. Lett. 369 (2003) 165–172.
[45] H. Okamoto, M. Ogura, T. Nakabayashi, M. Tasumi, Sub-picosecond excited-state dynamics of a carotenoid (spirilloxanthin) in the light-harvesting systems of *Chromatium vinosum*. Relaxation process from the optically allowed S_2 state, Chem. Phys. 236 (1998) 309–318.
[46] E. Papagiannakis, J.T. Kennis, I.H. van Stokkum, R.J. Cogdell, R. van Grondelle, An alternative carotenoid-to-bacteriochlorophyll energy transfer pathway in photosynthetic light harvesting, Proc. Natl. Acad. Sci. U. S. A. 99 (2002) 6017–6022.
[47] E. Papagiannakis, S.K. Das, A. Gall, I.H.M. van Stokkum, B. Robert, R. van Grondelle, H.A. Frank, J.T.M. Kennis, Light harvesting by carotenoids incorporated into the B850 light-harvesting complex from *Rhodobacter sphaeroides* R-26.1: excited-state relaxation, ultrafast triplet formation, and energy transfer to bacteriochlorophyll, J. Phys. Chem. B 107 (2003) 5642–5649.
[48] T. Polivka, D. Niedzwiedzki, M. Fuciman, V. Sundstrom, H.A. Frank, Role of B800 in carotenoid-bacteriochlorophyll energy and electron transfer in LH2 complexes from the purple bacterium *Rhodobacter sphaeroides*, J. Phys. Chem. B 111 (2007) 7422–7431.
[49] T. Polivka, T. Pullerits, H.A. Frank, R.J. Cogdell, V. Sundstrom, Ultrafast formation of a carotenoid radical in LH2 antenna complexes of purple bacteria, J. Phys. Chem. B 108 (2004) 15398–15407.
[50] J.P. Zhang, R. Fujii, P. Qian, T. Inaba, T. Mizoguchi, K. Onaka, Y. Watanabe, H. Nagae, Y. Koyama, Mechanism of the carotenoid-to-bacteriochlorophyll energy transfer via the S_1 state in the LH2 complexes from purple bacteria, J. Phys. Chem. B 104 (2000) 3683–3691.
[51] A.N. Macpherson, J.B. Arellano, N.J. Fraser, R.J. Cogdell, T. Gillbro, Efficient energy transfer from the carotenoid S_2 state in a photosynthetic light-harvesting complex, Biophys. J. 80 (2001) 923–930.
[52] T. Polivka, D. Zigmantas, J.L. Herek, Z. He, T. Pascher, T. Pullerits, R.J. Cogdell, H.A. Frank, V. Sundstrom, The carotenoid S_1 state in LH2 complexes from purple bacteria *Rhodobacter sphaeroides* and *Rhodopseudomonas acidophila*: S_1 energies, dynamics, and carotenoid radical formation, J. Phys. Chem. B 106 (2002) 11016–11025.
[53] R.Z.B. Desamero, V. Chynwat, I. van der Hoef, F.J. Jansen, J. Lugtenburg, D. Gosztola, M.R. Wasielewski, A. Cua, D.F. Bocian, H.A. Frank, Mechanism of energy transfer from carotenoids to bacteriochlorophyll: light-harvesting by carotenoids having different extents of pi-electron conjugation incorporated into the B850 antenna complex from the carotenoidless bacterium *Rhodobacter sphaeroides* R-26.1, J. Phys. Chem. B 102 (1998) 8151–8162.
[54] A. Angerhofer, R.J. Cogdell, M.F. Hipkins, A spectral characterization of the light-harvesting pigment–protein complexes from *Rhodopseudomonas acidophila*, Biochim. Biophys. Acta 848 (1986) 333–341.
[55] D. Zigmantas, R.G. Hiller, F.P. Sharples, H.A. Frank, V. Sundstrom, T. Polivka, Effect of a conjugated carbonyl group on the photophysical properties of carotenoids, Phys. Chem. Chem. Phys. 6 (2004) 3009–3016.
[56] T. Ritz, A. Damjanovic, K. Schulten, J.P. Zhang, Y. Koyama, Efficient light harvesting through carotenoids, Photosynth. Res. 66 (2000) 125–144.
[57] A.V. Ruban, R. Berera, C. Ilioaia, I.H.M. van Stokkum, J.T.M. Kennis, A.A. Pascal, H. van Amerongen, B. Robert, P. Horton, R. van Grondelle, Identification of a mechanism of photoprotective energy dissipation in higher plants, Nature 450 (2007) 575–578.
[58] R. Berera, I.H.M. van Stokkum, S. d'Haene, J.T.M. Kennis, R. van Grondelle, J.P. Dekker, A mechanism of energy dissipation in cyanobacteria, Biophys. J. 96 (2009) 2261–2267.
[59] H. Staleva, J. Komenda, M.K. Shukla, V. Slouf, R. Kana, T. Polivka, R. Sobotka, Mechanism of photoprotection in the cyanobacterial ancestor of plant antenna proteins, Nat. Chem. Biol. 11 (2015) 287–291.
[60] A. Freiberg, M. Ratsep, K. Timpmann, G. Trinkunas, N.W. Woodbury, Self-trapped excitons in LH2 antenna complexes between 5 K and ambient temperature, J. Phys. Chem. B 107 (2003) 11510–11519.
[61] M.A. Bopp, Y.W. Jia, L.Q. Li, R.J. Cogdell, R.M. Hochstrasser, Fluorescence and photobleaching dynamics of single light-harvesting complexes, Proc. Natl. Acad. Sci. U. S. A. 94 (1997) 10630–10635.
[62] T. Pflock, M. Dezi, G. Venturoli, R.J. Cogdell, J. Kohler, S. Oellerich, Comparison of the fluorescence kinetics of detergent-solubilized and membrane-reconstituted LH2 complexes from *Rps. acidophila* and *Rb. sphaeroides*, Photosynth. Res. 95 (2008) 291–298.
[63] R. Fujii, K. Onaka, M. Kuki, Y. Koyama, Y. Watanabe, The $2A_g^-$ energies of all-*trans*-neurosporene and spheroidene as determined by fluorescence spectroscopy, Chem. Phys. Lett. 288 (1998) 847–853.

[64] J.P. Zhang, T. Inaba, Y. Watanabe, Y. Koyama, Excited-state dynamics among the $1B_u^+$, $1B_u^-$ and $2A_g^-$ states of all-*trans*-neurosporene as revealed by near-infrared time-resolved absorption spectroscopy, Chem. Phys. Lett. 332 (2000) 351–358.
[65] F.S. Rondonuwu, Y. Watanabe, R. Fujii, Y. Koyama, A first detection of singlet to triplet conversion from the $1^1B_u^-$ to the 1^3A_g state and triplet internal conversion from the 1^3A_g to the 1^3B_u state in carotenoids: dependence on the conjugation length, Chem. Phys. Lett. 376 (2003) 292–301.
[66] Z.D. Pendon, G.N. Gibson, I. van der Hoef, J. Lugtenburg, H.A. Frank, Effect of isomer geometry on the steady-state absorption spectra and femtosecond time-resolved dynamics of carotenoids, J. Phys. Chem. B 109 (2005) 21172–21179.
[67] H.A. Frank, R. Farhoosh, R. Gebhard, J. Lugtenburg, D. Gosztola, M.R. Wasielewski, The dynamics of the S_1 excited-states of carotenoids, Chem. Phys. Lett. 207 (1993) 88–92.
[68] R. Fujii, T. Ishikawa, Y. Koyama, M. Taguchi, Y. Isobe, H. Nagae, Y. Watanabe, Fluorescence spectroscopy of all-*trans*-anhydrorhodovibrin and spirilloxanthin: detection of the $1B_u^-$ fluorescence, J. Phys. Chem. A 105 (2001) 5348–5355.